

LANL Salt International Update

Fuel Cycle Research & Development

*Prepared for
U.S. Department of Energy
Used Fuel Disposition Campaign
Milestone M4SF-18LA010303041*

*P.J. Johnson
S. Otto
D.J. Weaver
B. Dozier
T.A. Miller
A.B. Jordan
N.G. Hayes-Rich
P.H. Stauffer*

*Los Alamos National Laboratory
September 30, 2018*

Los Alamos National Laboratory Document
LA-UR-18-29105



DISCLAIMER

This information was prepared as an account of work sponsored by an agency of the U.S. Government. Neither the U.S. Government nor any agency thereof, nor any of their employees, makes any warranty, expressed or implied, or assumes any legal liability or responsibility for the accuracy, completeness, or usefulness, of any information, apparatus, product, or process disclosed, or represents that its use would not infringe privately owned rights. References herein to any specific commercial product, process, or service by trade name, trade mark, manufacturer, or otherwise, does not necessarily constitute or imply its endorsement, recommendation, or favoring by the U.S. Government or any agency thereof. The views and opinions of authors expressed herein do not necessarily state or reflect those of the U.S. Government or any agency thereof.

FCT Quality Assurance Program Document

Appendix E FCT Document Cover Sheet

Name/Title of Deliverable/Milestone		LANL Salt International Update		
Work Package Title and Number		SF-18LA01030304	Salt International Collaborations LANL	
Work Package WBS Number		1.08.01.03.03 - Salt Disposal R&D		
Responsible Work Package Manager		Philip H. Stauffer		
Date Submitted		(Name/Signature)		
Quality Rigor Level for Deliverable/Milestone	<input checked="" type="checkbox"/> QRL-3	<input type="checkbox"/> QRL-2	<input type="checkbox"/> QRL-1 <input type="checkbox"/> Nuclear Data	<input type="checkbox"/> N/A*
This deliverable was prepared in accordance with		Los Alamos National Laboratory (Participant/National Laboratory Name)		
QA program which meets the requirements of				
<input checked="" type="checkbox"/> DOE Order 414.1 <input type="checkbox"/> NQA-1-2000				
This Deliverable was subjected to:				
<input type="checkbox"/> Technical Review		<input type="checkbox"/> Peer Review		
Technical Review (TR)		Peer Review (PR)		
Review Documentation Provided		Review Documentation Provided		
<input type="checkbox"/> Signed TR Report or,		<input type="checkbox"/> Signed PR Report or,		
<input type="checkbox"/> Signed TR Concurrence Sheet or,		<input type="checkbox"/> Signed PR Concurrence Sheet or,		
<input checked="" type="checkbox"/> Signature of TR Reviewer(s) below		<input type="checkbox"/> Signature of PR Reviewer(s) below		
Name and Signature of Reviewers				
Hari Viswanathan				

*Note: In some cases there may be a milestone where an item is being fabricated, maintenance is being performed on a facility, or a document is being issued through a formal document control process where it specifically calls out a formal review of the document. In these cases, documentation (e.g., inspection report, maintenance request, work planning package documentation or the documented review of the issued document through the document control process) of the completion of the activity along with the Document Cover Sheet is sufficient to demonstrate achieving the milestone. QRL for such milestones may be also be marked N/A in the work package provided the work package clearly specifies the requirement to use the Document Cover Sheet and provide supporting documentation.

Table of Contents

List of Figures	V
List of Tables	VII
EXECUTIVE SUMMARY	1
1. ABSTRACT.....	6
2. INTRODUCTION.....	7
3. EXPERIMENTAL DESIGN	9
4. EXPERIMENTAL RESULTS.....	15
4.1 Porosity calculation for Run-of-Mine salt	17
5. NUMERICAL MODEL FORMULATION	17
6. SIMULATION DOMAIN, BOUNDARY CONDITIONS, AND APPROACH.....	22
6.1 Model calibration approach.....	24
6.2 Sensitivity simulation approach.....	25
6.2.1 RoM saturation sensitivity	25
6.2.2 DRZ saturation sensitivity	26
6.2.3 Relative capillary strength sensitivity	27
6.2.4 Time after drift opening	28
7. SIMULATION RESULTS.....	29
7.1 Model calibration: Simulations of a 15-day heating period	29
7.2 Sensitivity simulation results	32
8. DISCUSSION AND CONCLUSION.....	36
9. ACKNOWLEDGEMENTS	39
10. REFERENCES	40
APPENDIX A: SLIDES FOR INTERPORE PRESENTATION	44
APPENDIX B: ADDITIONAL EXPERIMENT INFORMATION.....	61
ROM experiment schematics and images.....	61
Instrument locations.....	64
Temperature data from instruments.....	66
Notes collected during experiment	71

List of Figures

Figure 1: Schematic of the heater assembly, provided by RESPEC Mining and Energy (Stoller Inc., 2014).	11
Figure 2: End view (left) and side view (right) of heater assembly marking locations on canister of heater strips. Note that the heaters extent most of the length of the canister in the side view. Active heaters for the experiment are THEA01, 02, and 03.	12
Figure 3: External view of complete canister assembly, placed on drift floor of WIPP prior to addition of RoM salt pile.....	12
Figure 4: (A) End view schematic of canister in salt pile, looking north along the centerline of the canister. Red lines indicate thermocouple arrays. The top and right-hand sides of the pile are surrounded by air. Below and left of the pile is the damaged rock zone (DRZ). (B) 2D mesh and end view of 3D mesh generated for numerical modeling. Red color indicates air; green is RoM salt; light blue is DRZ salt; dark blue is intact rock; canister shown with orange circle. Y-axis corresponds with north-south direction; x-axis corresponds to east-west direction. West is to left.	14
Figure 5: (A) Temperature of each point of thermocouple array in transect extending vertically upward from canister center. TSUR03 is thermocouple at top of canister. TROM numbers increase with distance from canister, with 5.08 cm (2 inch) spacing between measurements. Temperature stabilizes after about 15 days (vertical dashed line), excluding a minor drop during a WIPP power outage. (B) Temperatures at canister boundary and ends of thermocouple arrays after 90 days. Points mark location of corresponding measurement within pile. Red lines indicate thermocouple arrays as in Figure 1-A.	16
Figure 6: Temperature profile in small-diameter borehole beneath heater canister.	31
Figure 7: Comparison of simulation results (red) to experimental results (black) for measurement points on top and sides of canister. RoM indicates thermocouple measurement positioned 0.3048 m (1 foot) away from canister, in RoM salt pile.	32
Figure 8: Sum of absolute value of porosity changes in pile (Ψ) resulting from different parameters. (A, B, and C) Example porosity effects with increasing Ψ . (D) RoM saturation; (E) Initial DRZ saturation; (F) Ratio of strength of maximum capillary effects in RoM salt vs. DRZ; (G) Elapsed time between opening of drift and placement of canister.	35
Figure 9: Initial schematic of experiment setup. Circle in center is canister. Red lines indicate thermocouple arrays for temperature. Numbers are dimensions in inches.	62
Figure 10: End view of revised schematic, similar to initial schematic but with flattened top of pile extended to wall (top), and constructed ROM salt pile (bottom).....	63
Figure 11: ROM arrays (red) around canister. Numbers indicate designation for thermocouples as shown in Figures 12 and 13-17.	64
Figure 12: Thermocouple arrays with designators for subsequent data. TROM indicates arrays placed in ROM salt pile; TSAL arrays are placed in the intact salt of the floor; and TSUR are on the surface of the canister.....	65
Figure 13: Temperature measurements for transect extending vertically upward from canister. Thermocouple labels are shown as in Figure 12.	66

Experiments and Modeling to Support Field Test Design

Figure 14: Temperature measurements for transect extending laterally west (left in Figures 10 and 12) from canister. Thermocouple labels are shown as in Figure 12.	67
Figure 15: Temperature measurements for transect extending laterally east (right in Figures 10 and 12) from canister. Thermocouple labels are shown as in Figure 12.	68
Figure 16: Temperature measurements for transect extending vertically beneath canister. Thermocouple labels are shown as in Figure 12.	69
Figure 17: Temperature transects for pile top (black), west (red, left on Figures 10 and 12), and east (green, right on Figures 10 and 12).	70
Figure 18: Location of temperature measurements.....	72

List of Tables

Table 1: Base case simulation parameters. Highlighted values indicate parameters that are varied to improve model fit.....	25
Table 2: Parameters for RoM saturation sensitivity studies.....	26
Table 3: Parameters for DRZ saturation studies.	27
Table 4: Parameters for capillary strength sensitivity studies.	28

EXECUTIVE SUMMARY

This milestone presents material relating to international salt investigations during the 2018 fiscal year. Overall salt efforts this year were divided between the currently in-progress borehole experiments (see test plan TP-18-001, rev. 0 and DOE Milestone M3SF-18LA010303014), model development (see DOE milestone M3SF-18LA010303015), and validation of numerical modeling for generic salt repository applications domestically (intranational) and abroad (international). The present milestone focuses on the last of these subject areas. Work for international dissemination was conducted during the first half of the 2018 fiscal year and includes two international conference presentations—Geological Society of America (GSA) and the International Society for Porous Media (IntePore)—and a manuscript which is currently in review in Vadose Zone Journal. The prepared manuscript for Vadose Zone Journal is reproduced below in Sections 1-10. Slides for the GSA and InterPore presentations are similar, and the InterPore slides are reproduced in Appendix A. In Appendix B we present supplemental information related to the canister operation test.

During the 2018 fiscal year, research has aimed to improve understanding of physical processes in the Run-of-mine (RoM) salt surrounding heat-generating nuclear waste (HGNW) canisters in salt repositories when the *in-drift* disposal concept is applied. These efforts include experiments to directly examine changes in RoM salt when heated. In addition, numerical simulations using the porous flow code Finite Element Heat and Mass (FEHM; <https://fehm.lanl.gov>) have been conducted for model validation, calibration, and for prediction of experimental outcomes. Testing and improvement of FEHM can serve to improve numerical modeling in other porous flow codes, particularly the parallelized simulator PFLOTTRAN (<https://www.pfлотran.org/>). To these ends, we present numerical simulations of an ongoing

Experiments and Modeling to Support Field Test Design

heated single-canister experiment at WIPP, analysis of results to date, and possible constraints on the range of responses to HGNW sources in future international salt repositories. A new capillary retention function and updated mesh are used in these latest simulations.

Prior to the experiment, numerical simulations suggested that there was a possibility of extensive thermal-hydraulic-chemical (THC) reactions within the RoM salt pile surrounding the heated canister. These changes would be produced by either the evaporation of brine and precipitation of salt, or the condensation of fresh water out of water vapor and its consequent dissolution of salt. In settings where these reactions were continuous, porosity and permeability changes could be produced in the RoM salt pile that would affect the ability of brine to penetrate to the canister. Continuous reactions of this form are contingent on scenario, described in Johnson et al. (2017a), is that a rind of dense, low-porosity, impermeable salt would form around the canister while the distal portions of the pile degraded due to the condensation/dissolution processes. An alternative scenario under consideration is that insufficient brine recharge would occur to the heat source to drive the continuous reactions in the salt. Heat from the canister would simply vaporize the liquid brine near the canister and then the reaction would cease. These two scenarios carry divergent implications for the isolation, shielding, and containment surrounding emplaced canisters in the early time following emplacement of the HGNW canisters.

Model calibration is accomplished by simulating the first 15 days of canister heating. In the physical experiment, temperatures roughly leveled off at this time, with an overall long-term slight temperature decrease through the winter months before a rebound began during the summer heating period. Numerical simulations were constructed to match this early heating period and the long-term temperature trend, allowing estimation of material properties. These

Experiments and Modeling to Support Field Test Design

inferred parameters were then applied to a series of 365-day simulations to examine the long-term response of the RoM salt given variable initial conditions. We also evaluate the influence of several potentially important parameters to attempt to constrain the range of RoM salt effects and what processes may require further investigation. Variables of interest are the initial saturation of the RoM salt and the disturbed rock surrounding the drift, the strength of capillary action drawing water into the pile, and the elapsed time between opening of the drift and emplacement of the heat source and RoM salt. This last parameter relates directly to the brine content in the walls of the drift as well as the pressure decrease in the walls over time as the deep, hydrostatic brine is exposed to and equilibrates with atmospheric pressure air.

Based on the experiment to date and our updated simulations, extensive THC reactions are not occurring in the active experiment, and are unlikely in future scenarios. Our sensitivity analyses indicate that the greatest variability in effects relates to the saturation of the RoM salt that is placed around the heater. Additional changes may occur if waste is emplaced immediately after excavation of a drift, before pressure equilibration and drainage of the walls surrounding the drift occurs, but it is unlikely that waste would realistically be placed in such a drift within the short period of time necessary to limit these effects. Heat pipe-type interactions necessary to cause extensive RoM degradation are apparently unlikely in a ventilated drift. Instead, a chimney effect occurs in which air and its contained moisture is rapidly advected out of the pile. Insufficient moisture is returned to the RoM salt pile to cause further reactions.

Continuation of this work is planned for the late 2018 fiscal year and early 2019 fiscal year. The proposed work includes excavation of the salt pile, further model validation, and the incorporation of brine generation/release results from the ongoing borehole experiments in the walls of WIPP. Heat input to the experimental canister was first halved and then deactivated

Experiments and Modeling to Support Field Test Design

during the summer of 2018. Analysis of this portion of the experiment has not yet been conducted due to prioritization of the borehole experiments, but is planned during the autumn of 2018. The RoM pile will also be excavated during the autumn months if time and resources allow. These experimental results and associated simulations will be presented at the 2019 Waste Management conference. If feasible, an additional peer-reviewed manuscript will be produced during the early 2019 fiscal year.

Heat generating nuclear waste in salt: field testing and simulation

*Peter J. Johnson^{*1}, Shawn Otto², Douglas J. Weaver², Brian Dozier², Terry A. Miller¹, Amy B. Jordan³, Nathan G. Hayes-Rich¹, Philip H. Stauffer¹*

**Corresponding author: Peter J. Johnson, MS T003, Los Alamos National Laboratory, Los Alamos, NM 87545. Tel.: (505) 667-5518, Email: pjjohnson@lanl.gov*

¹EES-16: Computational Earth Science, MS T003, Los Alamos National Laboratory, Los Alamos, NM 87545

²Los Alamos National Laboratory Carlsbad Field Office, Carlsbad, NM 88221

³Neptune and Company, Lakewood, CO 80215

CORE IDEAS

- **A field-scale experiment and supporting numerical simulations are in progress to establish the response of salt backfill in an in-drift nuclear waste disposal setting**
- **Numerical simulations produce a close match of temperature around and under the piled salt backfill**
- **Thermal conductivity through the backfill appears constant, indicating that dissolution/precipitation reactions are not causing strong changes around the heat source**
- **Numerical simulations based on parameters estimated from the experiment suggest that degradation or alteration of salt backfill surrounding a heat source are unlikely to occur if the drift is allowed to dry and depressurize for a short time following excavation**

1. ABSTRACT

Investigations relating to in-drift disposal of heat-generating nuclear waste in salt have raised questions about heat/brine interactions in the unsaturated run-of-mine (RoM) salt pile used as backfill. These interactions have the potential to change the structure of the RoM salt surrounding the canister, possibly altering long-term containment of the source. An experiment is in progress at the Waste Isolation Pilot Plant (WIPP), New Mexico, USA, in which a heated canister is placed on the floor of an open drift, covered in a pile of RoM salt, and energized with 1000 watts. Temperature in the RoM salt pile has stabilized after about 15 days, allowing evaluation of the heat-up period of the ongoing experiment. Using a multiphase porous flow simulator that has been modified to handle salt specific coupled processes, we examine coupled thermal-hydrological-chemical behavior in the RoM salt pile. Our simulations suggest that for the relatively dry cases examined, porosity changes within RoM salt in a generic salt repository are likely to be minor. The primary sensitivity for porosity change is to the early moisture content of the RoM salt used to cover the canister. Secondary influences include moisture availability from the disturbed rock zone (DRZ) surrounding the drift and the capillary pressure ratio between the DRZ and the RoM salt. Porosity changes can be limited by using the driest possible RoM salt to cover the canister and by allowing the wall of the drift to drain for a period of time before emplacing canisters of HGNW and RoM salt.

2. INTRODUCTION

Geologic disposal of high level heat-generating nuclear waste (HGNW) remains a primary conceptual pathway to ensure the long-term safety and security of disused nuclear materials. Bedded salt has been a material of interest since at least 1957 (Hess et al., 1957) because it has numerous properties that are expected to aid in the containment and isolation of nuclear waste, e.g. viscoplastic closure of fractures, low porosity and permeability, and high thermal conductivity (Hansen and Leigh, 2011). More recently, studies pertaining to nuclear waste disposal in salt have been conducted in Germany (Brewits and Rothfuchs, 2007; Fahland and Heusermann, 2013; Wollrath et al., 2014) and in the United States at the Waste Isolation Pilot Plant (WIPP; see Rechar, 2000), the location for the present study. A primary goal of ongoing international efforts is to establish the safety case for bedded salt as a potential host material for high-activity HGNW.

One proposed concept for HGNW emplacement in salt is referred to as *in-drift* disposal (Washington Savannah River Company et al., 2008; Carter et al., 2011; Hansen and Leigh, 2011; Robinson et al., 2012). A horizontal tunnel, in context called a drift, is carved into the rock salt layer. A canister containing the HGNW is placed on the floor of this drift and covered with crushed run-of-mine (RoM) salt for shielding. After filling with waste canisters, the drift is backfilled with RoM salt. Viscoplastic closure of any remaining voids in the drift follows naturally (Hess et al., 1957; Rechar, 2000; Hansen and Leigh, 2011) and reduces the potential for migration of radioactive material.

Recent studies pertaining to the in-drift disposal concept identified a need to improve the current understanding of constitutive relationships in both RoM and solid salt in order to better constrain the long-term safety case for HGNW in any future salt repository (Callahan et al.,

2012; Stauffer et al., 2015; Hansen et al., 2017). One important uncertainty related to the in-drift concept concerns heating-induced changes in the RoM salt pile that alter brine and water vapor flow near the canister and could impact performance through changes to the mechanical properties of the RoM salt backfill (Stauffer et al., 2015). A series of field-scale tests was proposed which aim to examine this and related topics (DOE CBFO, 2012; Stauffer et al., 2013; Jordan et al., 2015a,b,c; Stauffer et al., 2015; Bourret et al., 2016; Johnson et al., 2017). An operational test of one of these experiments is currently underway and is the subject of this paper. This experiment features a stainless steel canister containing a heater assembly, representing a mock-up of a HGNW canister.

Data from the operational test can be used to examine the changes in the RoM salt resulting from multiphase flow interactions (Faghri, 1995; Olivella et al., 2011; Jordan et al., 2015a) within the salt pile. Evaporation of brine near the heat source triggers precipitation of salt and closure of porosity and reduction of permeability, while condensation of moisture in cooler areas leads to dissolution of salt and increases in porosity and permeability (Jordan et al., 2015a; Olivella et al., 2011; Blanco-Martin et al., 2018). Dissolution/precipitation reactions resulting from evaporation and condensation of brine (Olivella et al., 2011; Bourret et al., 2017; Johnson et al., in review) may strongly affect fluid flow to and around the waste canister. Based on this conceptual model and prior experimental work, heat/brine/vapor/salt interactions near the canister are hypothesized to result in one of two outcomes: (1) evaporation of brine near the canister and the creation of a dry halo around the heat source, with inadequate brine recharge to the heater to cause strong porosity and permeability effects (Hansen and Leigh, 2011), or (2) brine recharge to the heat source, porosity and permeability changes throughout the RoM salt pile, and potential impacts on the canister (Stauffer et al., 2013; Bourret et al., 2017; Johnson et

al., 2017a). Multiphase flow and material changes in repository salt are complex and are being explored through a variety of approaches, including coupling of thermal, hydrological, mechanical, and chemical processes (Birkholzer et al., 2004; Caporuscio et al., 2013; Kuhlman and Malama, 2013; Bourret et al., 2016; Rutqvist et al., 2016; Johnson et al., 2017b). The work herein focuses on the impacts of coupling thermal convection, multiphase liquid/vapor flow, and chemical precipitation/dissolution reactions.

In this paper, we report results from simulations of an in-progress heated canister experiment at WIPP using the Los Alamos National Laboratory porous flow simulator FEHM (Finite Element Heat and Mass; <https://fehmn.lanl.gov>; Zyvoloski et al., 2012). FEHM has been recently modified to include salt specific reactions (Stauffer et al., 2013; Jordan et al., 2015a,b,c; Bourret et al., 2016; Johnson et al., 2017a). First, we provide an independent estimate of porosity in the RoM salt pile and calibrate our numerical simulation of the first 15 days of heating based on early temperature results. We then present simulations exploring sensitivity of the system to changes in porosity over 100 days of heating. These simulations are designed to illuminate the relative importance of poorly constrained parameters including 1) the initial saturation of the RoM salt, 2) the saturation of the disturbed rock zone (DRZ), 3) the capillary pressure ratio between the DRZ and the RoM salt, and 4) the elapsed time between opening of the drift and placement of the waste package. Finally, results are discussed with respect to planning and implementation at possible future high level waste repositories in bedded salt formations.

3. EXPERIMENTAL DESIGN

The experiment features a stainless steel cylindrical canister with internal heating elements (Figure 1), placed on the floor of a 2.44 m (8 feet) tall drift in bedded salt. This

Experiments and Modeling to Support Field Test Design

canister is a mock-up of a standard Savannah River HGNW canister and is designed to operate in the hostile WIPP environment. High temperatures, saline brine, and acid gas generation all can cause corrosion of equipment. An assembly inside the canister contains six strip heaters, each capable of outputting 600W. Three of these heaters are designed to operate as a primary array, with the other three included as a secondary backup array. The heater canister is 2.67 m (8.75 feet) long with a radius of 0.3048 m (1 foot) and is oriented with its long axis in the north-south direction. The interior of the canister is filled with ceramic, spherical sand (cerabeads) which are intended to represent thermal properties of vitrified nuclear waste (Jordan et al., 2015b). A total of 1000 watts are delivered electrically to the three heating elements located inside the canister. A programmable control system limits energy input at the heaters to the desired level. Heater strips are affixed to an inner sleeve assembly inserted inside the canister with centralizing spacers.

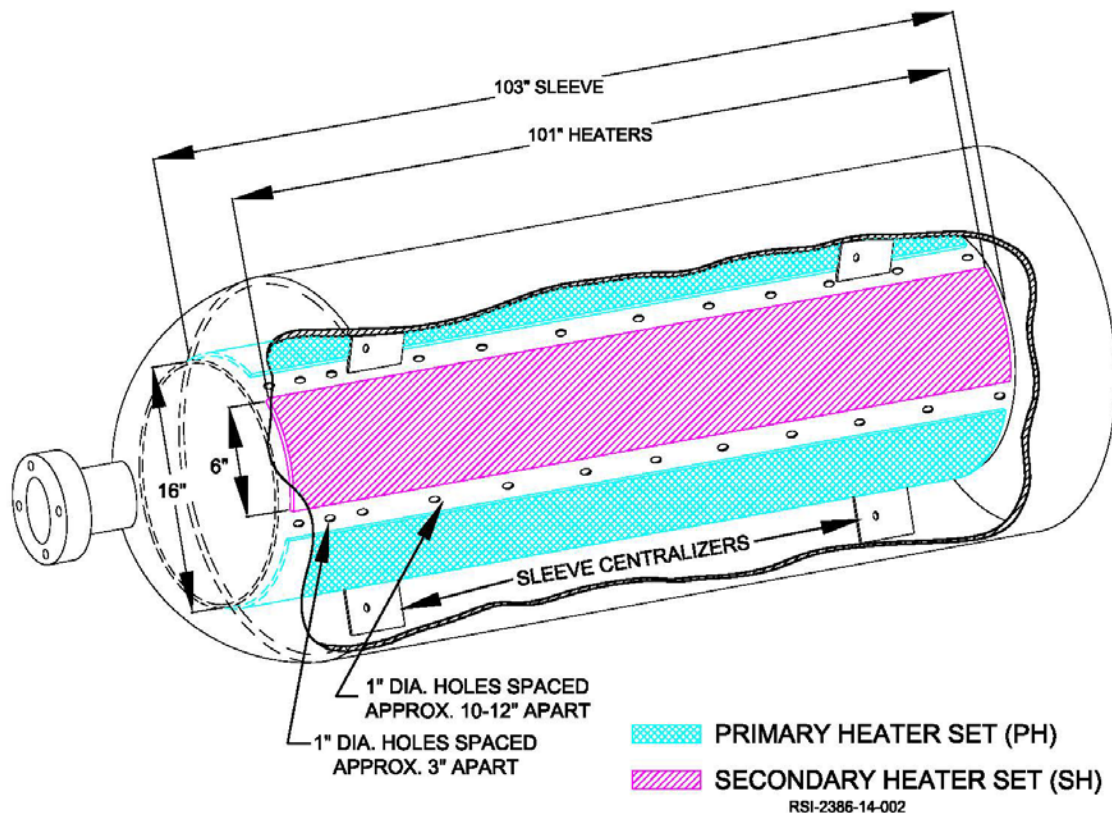
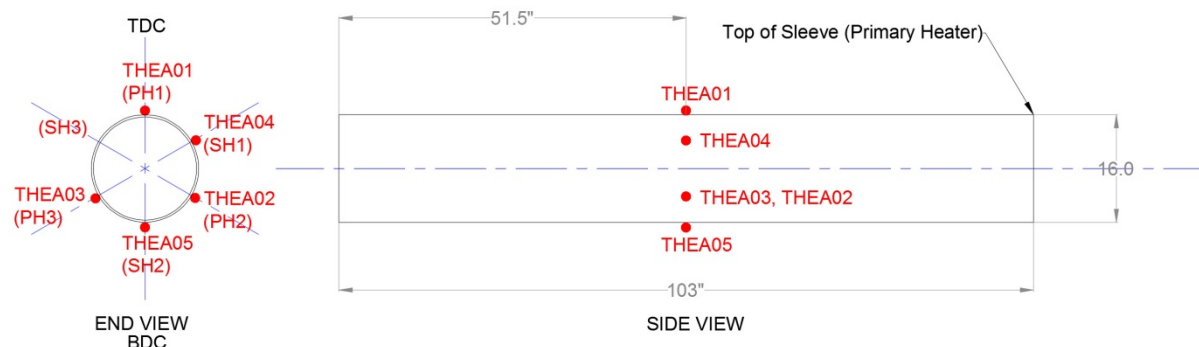


Figure 1: Schematic of the heater assembly, provided by RESPEC Mining and Energy (Stoller Inc., 2014).

The active heaters in the ongoing experiment are the primary array, monitored by thermocouples numbered THEA01, 02, and 03 in Figure 2. In the event of failure of these heaters, the secondary set could be activated. Testing of the heater was conducted in a separate set of experiments in 2014 (Stoller Inc., 2014; Jordan et al., 2015a). Figure 3 shows the outside appearance of the final canister setup as placed on the floor of WIPP.

TCs ON THE MIDPOINT OF THE STRIP HEATERS



THEA = Thermocouples on the heater strips inside the canister (1-5)

Figure 2: End view (left) and side view (right) of heater assembly marking locations on canister of heater strips. Note that the heaters extent most of the length of the canister in the side view. Active heaters for the experiment are THEA01, 02, and 03.



Figure 3: External view of complete canister assembly, placed on drift floor of WIPP prior to addition of RoM salt pile.

Experiments and Modeling to Support Field Test Design

The experiment is located in a horizontal shaft near a major entrance into WIPP that is tens of meters long and wide enough for vehicles to pass. Crushed RoM salt covers the canister and forms an asymmetric, flat-topped pile with downward sloping sides (Figure 4-A). The top of the pile is 0.9144 m (3 feet) above the center of the canister and 1.22 m (4 feet) above the floor of the drift. Thermocouple arrays are placed extending one canister-radius (0.3048 m) vertically (+z direction) and laterally ($\pm x$ -direction), with 5.08 cm (2 inch) spacing between measurement points. An additional thermocouple array is placed in a small-diameter borehole beneath the canister, and extends to 0.6096 m (2 feet) beneath the canister. Based on these measurements, a mesh was constructed for numerical simulations (Figure 4-B).

The walls of the drift consist of intact, bedded salt. WIPP salt is well characterized in general but shows localized heterogeneities in the rock salt, including small veins of clay, polyhalite, gypsum, fluid inclusions, fractures, and lithologic variability common in bedded evaporites (Powers et al., 1978; Krieg, 1984; Lappin, 1988). A disturbed rock zone (DRZ), also referred to as an excavation damage zone (EDZ; Tsang et al., 2015), extends into the wall from the open air of the drift. Fracture permeability and a small amount of additional porosity are formed in this region due to pressure unloading of the rock salt and vibrational damage from the mining process. Additional permeability in the DRZ may allow brine from the walls (McTigue and Nowak, 1987) of the drift to enter the RoM salt pile.

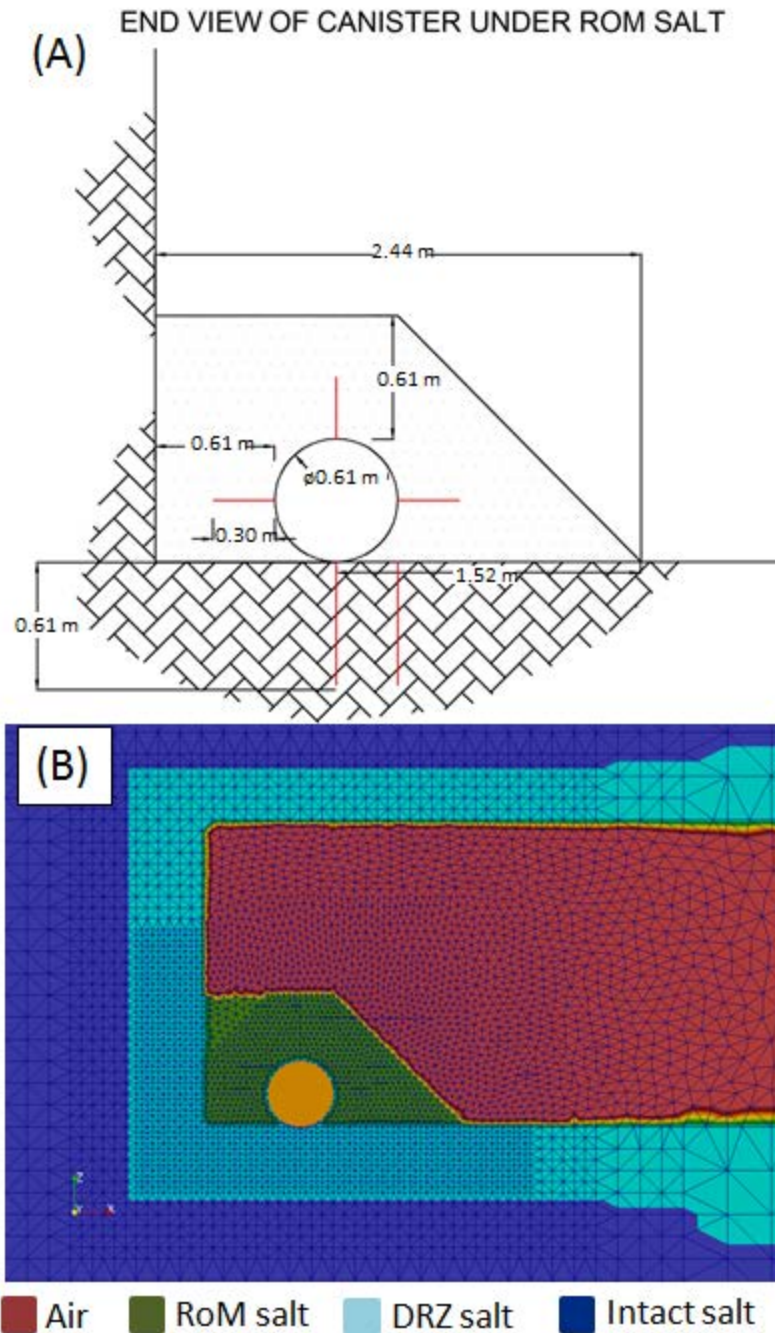


Figure 4: (A) End view schematic of canister in salt pile, looking north along the centerline of the canister. Red lines indicate thermocouple arrays. The top and right-hand sides of the pile are surrounded by air. Below and left of the pile is the damaged rock zone (DRZ). (B) 2D mesh and end view of 3D mesh generated for numerical modeling. Red color indicates air; green is RoM salt; light blue is DRZ salt; dark blue is intact rock; canister shown with orange circle. Y-axis corresponds with north-south direction; x-axis corresponds to east-west direction. West is to left.

4. EXPERIMENTAL RESULTS

The experiment was activated at 0915 mountain daylight time (1615 UTC) on 21 September 2017. Approximate steady state temperatures were attained after about 15 days (Figure 5-A). A brief power outage before 20 days can be seen as a drop in temperature in Figure 5-A. Similar temperature values and gradients above and lateral to the heater suggest a conduction-dominated system (Figure 5-B).

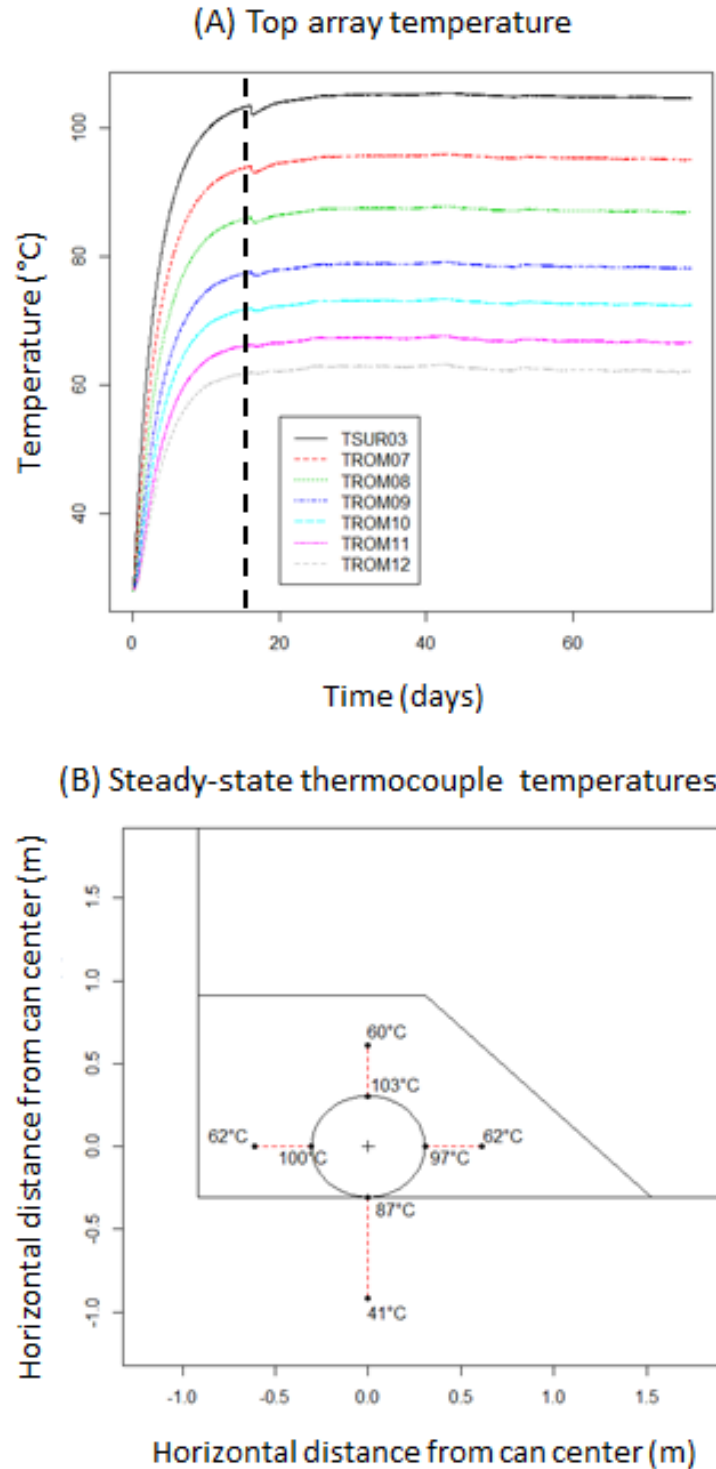


Figure 5: (A) Temperature of each point of thermocouple array in transect extending vertically upward from canister center. TSUR03 is thermocouple at top of canister. TROM numbers increase with distance from canister, with 5.08 cm (2 inch) spacing between measurements. Temperature stabilizes after about 15 days (vertical dashed line), excluding a minor drop during a WIPP power outage. (B) Temperatures at canister boundary and ends of thermocouple arrays after 90 days. Points mark location of corresponding measurement within pile. Red lines indicate thermocouple arrays as in Figure 1-A.

4.1 Porosity calculation for Run-of-Mine salt

Based on the thermal data from the experiment (Figure 5), an analytical solution for thermal conduction properties of the RoM salt pile can be developed assuming conductive heat transfer radial to a heated pipe,

$$\kappa = \frac{Q \ln(r_2/r_1)}{2\pi L(\Delta T)}, \quad (1)$$

where κ is thermal conductivity (W/m·K), Q is the heat input into the relevant canister length (75 watts for a 0.2 m long canister segment), r_2 and r_1 are the locations of the measurements radially to the center of the ring (0.6096 m and 0.3048 m respectively), L is the length of the canister segment (0.2 m), and ΔT is the difference in temperature at the two measurement points. Using an approximated temperature difference of 40°C from the canister wall (100°C to the 30.48 cm point (60°C) yields a thermal conductivity of about 1 W/m·K. Based on experiments at the Asse salt mine in Germany (Becthold et al., 2004), thermal conductivity of granular salt scales with porosity (Gable et al., 2009) as

$$\kappa_{T-ASSE}(n) = -270n^4 + 370n^3 - 136n^2 + 1.5n + 5 \quad (2)$$

This function is only valid for porosities up to about 0.4, but provides a match to the calculated thermal conductivity at a porosity of about 0.3.

5. NUMERICAL MODEL FORMULATION

Simulations of the salt domain are performed using the code Finite Element Heat and Mass (Zyvoloski et al., 2012). For the present problem, model functions and formulations to handle the chemistry of brine and salt and the effects of salt on the heat and mass transport are used (Stauffer et al., 2015; Johnson et al., in review). FEHM applies equations for conservation of water mass m , air mass η , and energy e between connected volume elements as:

Experiments and Modeling to Support Field Test Design

$$\frac{\partial A_m}{\partial t} + \nabla \cdot f_m + q_m = 0, \quad (5)$$

$$\frac{\partial A_\eta}{\partial t} + \nabla \cdot f_\eta + q_\eta = 0, \quad (6)$$

$$\frac{\partial A_e}{\partial t} + \nabla \cdot f_e + q_e = 0 \quad (7)$$

where A is the quantity (mass or energy), f is the flux, q is the source/sink term and t is time.

Water mass per unit volume A_m is given by

$$A_m = n(S_v \rho_v (1 - \eta_v) + S_l \rho_l (1 - \eta_l)) \quad (8)$$

And air mass per unit volume A_η is

$$A_\eta = n(S_v \rho_v \eta_v + S_l \rho_l \eta_l) \quad (9)$$

where S is the saturation and ρ the density of the vapor phase and liquid phase (subscripts v and l); n is porosity; and $\eta_{(v,l)}$ is the mass fraction of air contained in the vapor or liquid phase respectively.

Mass fluxes for water and air are:

$$f_m = (1 - \eta_v) \rho_v \bar{u}_v + (1 - \eta_l) \rho_l \bar{u}_l \quad (10)$$

and

$$f_\eta = n(\eta_v \rho_v \bar{u}_v + S_l \rho_l \bar{u}_l) \quad (11)$$

where \bar{u} is the volumetric flux. Darcy's Law controls the volumetric flux of the vapor and liquid,

$$\bar{u}_v = -\frac{k_{rv}}{\mu_v} (\nabla P_v - \rho_v g) \quad (12)$$

and

$$\bar{u}_l = -\frac{k_{rl}}{\mu_l}(\nabla P_l - \rho_l g) \quad (13)$$

where k_r is the relative permeability of the respective phases, P is pressure, and g is the gravitational vector. Relative permeability in the present simulations is a linear fit of saturation. Fluid density and viscosity are polynomial functions of pressure and temperature based on National Bureau of Standards data (Haar et al., 1984).

Energy per unit volume A_e is given as

$$A_e = (1 - n)\rho_r\gamma_r + n(S_v\rho_v\gamma_v + S_l\rho_l\gamma_l) \quad (14)$$

with $\gamma_r = C_{pr}T$, and the energy flux f_e given by

$$f_e = \rho_v h_v \bar{u}_v + \rho_l h_l \bar{u}_l - \kappa \nabla T \quad (15)$$

The subscript r refers to the solid phase; γ is the specific internal energy; C_{pr} is specific heat of the rock; h_v and h_l are specific enthalpies for the vapor and liquid phases; κ thermal conductivity; and T is temperature. Gravitational potential energy is embedded in the liquid phase specific enthalpy (or methalpy) definition (Stauffer et al., 2014) in FEHM when gravity is enabled as

$$h_l = C_p T + P_l V_l + gz \quad (16)$$

where C_p is the specific heat of the water, T temperature, P pressure, V_l is specific volume, and z is height above a reference in the direction away from the center of mass of the gravity field.

Thermal conductivity for non-salt portions of the model are specified by the user directly. Within the salt medium, thermal conductivity is a function both of temperature and porosity. The temperature dependence is based on Munson et al., (1990) as

$$\kappa_{T-WIPP}(T) = \kappa_{T-300} \left(\frac{300}{T} \right)^{1.14} \quad (17)$$

where T is temperature in kelvin and κ_{T-300} is the thermal conductivity of pure halite at 300 K ($5.4 \text{ Wm}^{-1}\text{K}^{-1}$). Porosity n and thermal conductivity are related based on the function of Gable et al., (2009), which was developed as a function fit to data from Bechtold et al., (2004), at the Asse salt mine in Germany. This function is

$$\kappa_{T-ASSE}(n) = -270n^4 + 370n^3 - 136n^2 + 1.5n + 5 \quad (18)$$

Above porosity values of $n \approx 0.4$, this function becomes unphysical. Consequently, we apply a linear decrease in thermal conductivity with increasing porosity, so that at $n = 1$ the thermal conductivity value is that of air. Temperature and porosity effects on thermal conductivity are combined by scaling κ_{T-ASSE} to match κ_{T-300} at $n = 0$,

$$\kappa_{T-300}(n) = \left(\frac{\kappa_{T-300}}{\kappa_{T-ASSE}(n=0)} \right) \times \kappa_{T-ASSE}(n) \quad (19)$$

In this case, $\kappa_{T-300} / \kappa_{T-ASSE}$ is 5.4/5.0 or 1.08.

FEHM salt functions (Harp et al., 2014; Stauffer et al., 2015; Bourret et al., 2016; Johnson et al., in review) include solubility of salt in water with temperature as derived from Sparrow (2003). Porosity changes are based on the transition of salt between liquid and solid phases. Precipitation of salt reduces porosity, while dissolution increases porosity; thus, porosity is updated in each chemistry iteration ic as

$$\Delta n_{ic} = -\Delta c \rho_s \frac{1}{\rho_{NaCl}} (1 - n_{ic}) \quad (20)$$

where Δc is the change of moles of solid salt per weight of the solid (kg), ρ_s is density of the solid (kg/m^3), M_s is the molar mass of the solid (kg/mol), and ρ_{NaCl} is the density of salt, with $\rho_s =$

ρ_{NaCl} . Permeability is related to porosity based on Cinar et al., (2006), constrained to lie between a maximum of 0.9999 and a minimum of 10^{-5} .

Water vapor diffusion accounts for thermal and pressure effects described by

$$D_{va} = \tau D_{va}^o (P_o/P) \left(\frac{T+T_o}{T_o} \right) 1.81 \quad (22)$$

where τ is tortuosity, $D_{va}^o = 2.23 \cdot 10^{-5} \text{ m}^2/\text{s}$, $T_o = 273.15 \text{ K}$, T is temperature ($^{\circ}\text{C}$), P is pressure (MPa), and $P_o = 0.1 \text{ MPa}$ (Pruess 1991). Water vapor pressure is a function of temperature and is lowered by the presence of salt and other additional materials in the WIPP setting (Bourret et al., 2016; Bourret et al., 2017). The effective free air water vapor diffusion coefficient is then modified based on the Millington-Quirk (1961) relationship. A modified tortuosity term for gas transport in porous media is applied (Ho and Webb, 1998; Stauffer et al., 2009),

$$\tau = (S_a n)^{7/3} / n^2 \quad (23)$$

Diffusive mass transport of water vapor through air is

$$f_{mwv} = -D_{va} n S_v W_{Mwv} \nabla C_{wv} \quad (24)$$

where f_{mwv} is the diffusive mass flux of water vapor, W_{Mwv} is the molecular weight of water vapor (kg/mol), and C_{wv} is the moles of water vapor per cubic meter. Non-condensable gas (air) is allowed to diffuse along its concentration gradient with a diffusive mass flux as:

$$f_{ma} = -D_{va} n S_v W_{Mwa} \nabla C_a \quad (25)$$

where f_{mwa} is the diffusive mass flux of air, W_{Ma} is the molecular weight of air (kg/mol), and C_{wa} is the moles of air per cubic meter.

Porosity effects are expressed using a porosity change severity index, ψ . This index is calculated as the sum of the magnitude of the porosity change at each node i ,

$$\Delta V = \sum_{i=1}^{\alpha} |dn_i| V_i \quad (26)$$

where α is the total number of nodes in the RoM salt pile, dn_i is the porosity change at a given node, and V_i is the volume represented by the node. The ratio of ΔV to the total pile volume V_t yields the index of the severity of porosity changes, ψ , as

$$\psi = \frac{\Delta V}{V_t} \quad (27)$$

Capillary effects in the RoM salt pile are simulated using a dynamic, porosity-dependent retention function (Johnson et al., 2017a; Johnson et al., in review). The function changes residual saturation and maximum capillary pressure at each timestep based on updated porosity, thereby strengthening capillary forces in nodes where porosity decreases and weakening them where porosity increases and pore diameters expand. Saturation-only retention functions can lead to unphysical results when porosity greatly increases, such as capillary pressure causing water to be retained in nodes where no actual porous medium remains. Accounting for porosity in the retention function prevents such issues.

6. SIMULATION DOMAIN, BOUNDARY CONDITIONS, AND APPROACH

Based on characterization of the experiment within WIPP, a thin (0.2 m) computational mesh (nominally 2-D) was developed (Figure 4-B), representing an east-west slice through the center of the canister. We adopt a Cartesian reference frame with the positive- x axis to the east, perpendicular to the long axis of the canister; the positive- y axis to the north, parallel to the long axis of the canister; and gravitational acceleration in the $-z$ direction. Overall dimensions of the

Experiments and Modeling to Support Field Test Design

domain are 18.7 m width (x direction), 0.2 m length (y direction), and 36.6 m height (+z direction). The canister center is at the origin and has a radius of 0.3048 m (1 ft.). The bottom of the canister contacts the floor of the simulated drift at a single node. RoM salt surrounds the canister as shown in the schematic (Figure 4-A). Air extends vertically above and laterally in the +x direction (east) surrounding the pile. The DRZ surrounds the open air of the drift and forms the bottom (-z) and left (-x) boundaries of the salt pile. Damage in the DRZ is expressed as a region with order-of-magnitude higher porosity and increased permeability following Jordan et al., (2015c).

A far-field rock boundary of constant 28°C and 10 MPa are assigned at the maximum-z, minimum-z, and minimum-x (top, bottom, and left) edges of the intact salt unit. A constant air pressure of 0.101 MPa is assigned to a node in the air region along the positive-x edge of the domain, slightly below the top of the simulated open drift. This boundary adds or removes gas as necessary to maintain the specified air pressure. In tandem with the air input, an additional boundary condition is applied at the higher-pressure air node, which specifies a fixed mixing ratio of air/water vapor, representing constant humidity. Water vapor mass is added or removed to maintain this specified mixing ratio at the boundary node. Based on the average annual temperature and humidity in WIPP (Bourret et al., 2017), this value is assigned to a constant 0.8906. A corresponding node of constant 0.100 MPa gas pressure is placed at the top of the air zone directly above the pile, inducing a flow of the specified humidity air across the top of the RoM salt pile to simulate the flow of ventilation air in the experimental drift. This combination of boundary conditions drives air at a fixed humidity through the drift and over the top of the pile, adding or removing water from the RoM salt. Temperature above the pile was not continuously measured, but sampling after the pile attained steady state indicates that air within a

few cm of the top of the pile remains within 0.01°C of ambient air elsewhere in the drift. Air in the simulations is therefore fixed to a constant 28°C .

For all scenarios presented, we begin with an isothermal background simulation to establish the initial condition of the pile emplacement, followed by a simulation with the heat source applied. Background simulations were typically run for 365 days of model time, except where otherwise described below. Finally, the full 100 day simulation with added heat was activated from the background condition. Simulations take between 2 and 48 hours to complete, with greater porosity redistribution leading to longer simulation times. In the current study, we describe a general range of results and simulation behaviors as parameters are varied. Reproducing more detailed experimental results with respect to porosity changes will be undertaken after excavation of the salt pile in late 2018.

6.1 Model calibration approach

Initial heating of the pile and the achievement of an approximate steady-state temperature in the experiment provide an opportunity to calibrate model simulations against the measured data. Matching the steady-state temperature in the simulations to the experiment allows estimation of thermal parameters and, to an extent, material properties within the crushed salt and the DRZ beneath the drift. Thus, we apply known material properties where possible to the model domain, such as those of stainless steel to the canister rim, thermal properties of cerabeads (Jordan et al., 2015a), and intact salt in the walls (Table 1). For the calibration presented in the results section, two remaining free parameters, thermal conductivity of the DRZ and RoM salt, are varied manually to improve the match between simulated and measured temperatures. In addition, we also modify thermal conductivity values of the nodes just beneath the simulated base of the canister and salt pile.

Table 1: Base case simulation parameters. Highlighted values indicate parameters that are varied to improve model fit.

Property	RoM salt	DRZ salt	Rock salt	Canister edge	Ceramic beads
Porosity (-)	0.3	0.01	0.001	10^{-5}	$10^{-5\dagger}$
Permeability (m^2)	10^{-12}	10^{-17}	10^{-20}	10^{-22}	10^{-22}
Density* (kg/m^3)	2165.0	2165.0	2165.0	8000.0	1690.0
Thermal conductivity ($\text{W}/\text{m}\cdot\text{K}$)	1.03	5.2	5.4	15.0	0.24
Specific heat capacity ($\text{MJ}/\text{kg}\cdot\text{K}$)*	931.0	931.0	931.0	500.0	100.0
Initial saturation (-)	0.01	0.1	1	10^{-6}	10^{-6}
Maximum Capillary pressure (MPa)	0.5	1.0	1.0	0.0	0.0

*Note that density and specific heat capacity are specified for the solid matrix and modified within the model by porosity and saturation for bulk material properties.

[†]Properties of the ceramic beads inside the canister were fit to data from an earlier experiment¹⁶.

6.2 Sensitivity simulation approach

We next describe a set of four primary sensitivity analyses designed to explore simulated porosity change in the RoM salt pile surrounding the heated canister during 100 days of heating.

6.2.1 RoM saturation sensitivity

The sensitivity of the simulated porosity change with respect to RoM saturation is examined by varying the initial saturation of the RoM pile from 0.001 to 0.1 (Table 2). This range is constrained by the volume of water available within the mined salt and its subsequent mass changes. Assuming dense rock salt (porosity = 0.001) is fully saturated, its volumetric water content (porosity \times saturation) would be 0.001. If that salt was ground up and deposited in a pile with a porosity of 0.3, the saturation of the resulting RoM salt pile would be about 0.003,

Experiments and Modeling to Support Field Test Design

close to our minimum estimate of 0.001. A maximum estimate is more difficult to constrain, but is likely to fall near the residual saturation of the material, which is unknown and likely variable. Prior experimental work (Olivella et al., 2011) determined a residual saturation value in fine granular salt of about 0.05. Allowing for some error from case to case, we estimate a maximum initial RoM saturation of 0.1. An evaporation pan experiment indicated that if relative humidity of the ambient air surpassed about 28%, a small mass of water would enter the pile, while any lower relative humidity value would dry the pile (Bourret et al., 2017). WIPP RoM salt is likely fairly dry as a result of the general low humidity near the air intake over the course of years. How these results would translate to other rock salt compositions and other locations is unknown.

Table 2: Parameters for RoM saturation sensitivity studies.

Parameter	Value
RoM saturation (-)	0.001, 0.01, 0.05, 0.1
DRZ saturation (-)	0.1
RoM maximum capillary strength* (MPa)	0.5
DRZ maximum capillary strength (MPa)	1.0
Background run time (days)	365

*Value varies over course of model run at each node; listed value is as initially specified

6.2.2 DRZ saturation sensitivity

The saturation of the DRZ is a major uncertainty and likely varies spatially at WIPP, depending both on geologic heterogeneity and the length of elapsed time between opening of the drift and emplacement of the radiogenic sources. We assume that the DRZ is initially fully saturated, and gradually desiccates as moisture is entrained into air passing through the repository. An additional complication is the potential generation of brine from mineral hydration and the release of trapped brine from pores in the salt. Experiments to further examine these topics are in development (Johnson et al., 2017b). We consider a range from 0.05 (possible residual saturation) to 1.0 (fully saturated) for the initial DRZ saturation (Table 3).

Table 3: Parameters for DRZ saturation studies.

Parameter	Value
RoM saturation (-)	0.01
DRZ saturation (-)	0.05, 0.1, 0.3, 0.5, 0.7, 1.0
RoM maximum capillary strength* (MPa)	0.5
DRZ maximum capillary strength (MPa)	1.0
Background run time (days)	365

*Value varies over course of model run at each node; listed value is as initially specified

6.2.3 Relative capillary strength sensitivity

Saturation of the DRZ impacts flow toward the RoM pile in two ways. First, increased DRZ saturation increases the amount of water available to the RoM salt pile. Second, increased DRZ saturation reduces the initial capillary pressure of the DRZ, allowing capillary forces to draw moisture into the RoM salt. In addition, the capillary strength of the dry RoM salt pile itself is of crucial importance because it may draw brine to the canister to replace evaporated moisture. Strong capillary effects within the DRZ will tend to counteract those of the RoM salt, retaining water in the DRZ instead of allowing it to enter the RoM salt pile. We therefore conduct two suites of sensitivity simulations to illuminate the role of capillary forces between the DRZ and the RoM salt pile. In the first, the DRZ is initially at its low default saturation, and the maximum initial capillary pressure of the dry RoM salt pile is varied (Table 4). In the second, the DRZ is initially fully saturated and RoM capillary effects are varied. These simulations place boundaries on the effects of varying capillary action by examining both the case of competing capillary forces and the effects of varying the magnitude of capillary forces at early time in the saturated-DRZ case.

Table 4: Parameters for capillary strength sensitivity studies.

Parameter	Value
RoM saturation (-)	0.01
DRZ saturation (-)	0.1 and 1.0
RoM maximum capillary strength* (MPa)	0.05, 0.07, 0.1, 0.3, 0.5, 1.0
DRZ maximum capillary strength (MPa)	1.0
Background run time (days)	365

*Value varies over course of model run at each node; listed value is as initially specified

6.2.4 Time after drift opening

Following the opening of a drift, several different processes are expected to occur simultaneously. As noted in the DRZ saturation study above, moisture in the DRZ will tend to be drawn into ambient air flowing through the facility. A low-pressure front will advance into the walls of the drift from the open air because the ~atmospheric pressure open air boundary is placed adjacent to fluids at hydrostatic or lithostatic pressure. We therefore select a pressure of 10 MPa for the DRZ as the starting point for these simulations. A background run is conducted in which the salt pile and canister are simulated using the same properties assigned to air (Table 1). The duration of this run represents the elapsed time between opening of the drift and emplacement of the pile (Table 5). After the background run completes, a new simulation is conducted in which initial conditions are read from the output of the previous simulation, and salt pile and canister properties are applied. As specified, the DRZ attains a steady state at about 60 days after which time little change in saturation or pressure occur.

Table 5: Parameters for study of time after drift opening.

Parameter	Value
RoM saturation (-)	0.01
DRZ saturation (-)**	1.0
DRZ liquid pressure (MPa)**	10.0
RoM maximum capillary strength* (MPa)	0.5
DRZ maximum capillary strength (MPa)	1.0
Background run time (days)	0, 1, 3, 5, 7, 10, 15, 30, 45, 60, 75, 90, 100, 365

*Value varies over course of model run at each node; listed value is as initially specified

**Initial value

7. SIMULATION RESULTS

7.1 Model calibration: Simulations of a 15-day heating period

Using the analytical estimate of $1 \text{ W/m}\cdot\text{K}$ for thermal conductivity of the pile and base case parameters from Table 1, we simulate 15 days of model time with constant material properties and compare the temperature of the node nearest the measurement points shown in Figure 4-B. Thermal conductivity of the DRZ and RoM units are varied manually to improve the temperature match and final values of these parameters are listed in Table 1. For these initial heating runs, the porosity change components of the model are not active and a fixed thermal conductivity value is used.

This calibrated simulation yields a close match to measured data (within 5°C) on the sides of the canister and in the RoM salt pile on either side (+x and -x direction from canister center). The initial heating rate above the canister is slightly higher in the simulations than in the experiment, although the two values converge after the first few days. Since the temperature divergence occurs from the beginning of the experiment/model time, and the thermocouple array does not show any long-term increases or decreases that would suggest changing thermal conductivity over time, the difference is unlikely to be produced by porosity changes from heat/brine interactions. Based on the overall close match of simulation and experiment temperature results, we elect to use the $\sim 1 \text{ W/m}\cdot\text{K}$ thermal conductivity value for subsequent simulations.

Although the base-case simulations are able to capture the temperature in the RoM salt pile quite well, the temperature profile in the floor beneath the canister shows a sudden sharp drop between the base of the canister and the first thermocouple (Figure 6) that is not seen in the base-case simulation. Furthermore, measured temperatures at the base of the canister are

Experiments and Modeling to Support Field Test Design

unexpectedly hot if we assume that the canister is in direct contact with intact, highly conductive salt ($> 5 \text{ W/m}\cdot\text{K}$). We believe that the elevated temperatures seen directly beneath the canister in the active experiment are related to the placement of the experiment near the WIPP air intake shaft. Material from higher stratigraphic layers travels down the intake shaft and leaves a layer of fine material on the floor. This material is not composed of salt. Consequently, the coupling between the canister and underlying intact salt is relatively poor in the experiment and the canister base is relatively well insulated. By allowing for slightly higher thermal conductivity within the pile and adding a thin insulating layer below the pile (about 2 cm), we were able to match temperatures beneath the pile to within 5°C (Figure 7). However, for the subsequent parameter sensitivity analysis, we elect to assume direct contact between the canister and the DRZ in the floor of the drift, as would be expected in an active disposal setting where outside dust has not been permitted to accumulate over decades.

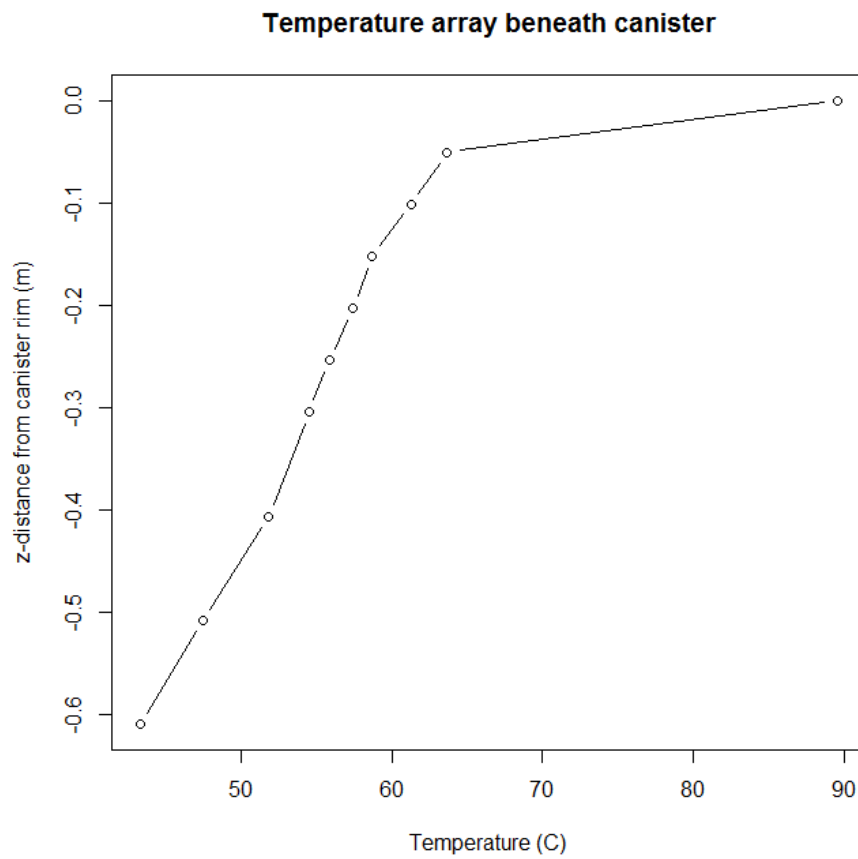


Figure 6: Temperature profile in small-diameter borehole beneath heater canister.

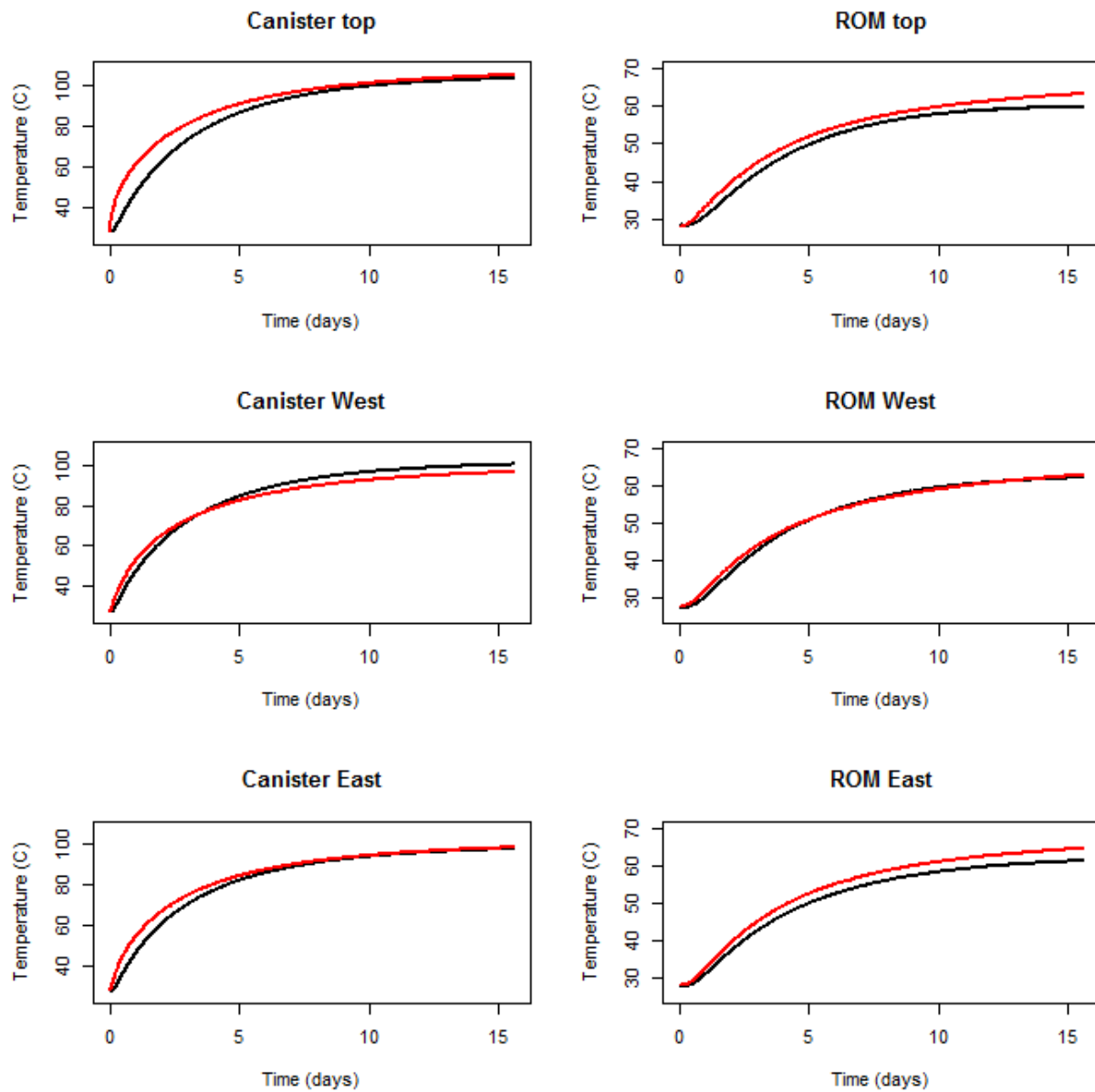


Figure 7: Comparison of simulation results (red) to experimental results (black) for measurement points on top and sides of canister. RoM indicates thermocouple measurement positioned 0.3048 m (1 foot) away from canister, in RoM salt pile.

7.2 Sensitivity simulation results

Although specific locations and magnitudes of porosity change vary between simulations, overall trends can be identified. An increased ψ value generally relates to the formation of a band of dissolution and precipitation along the junction of the RoM salt and DRZ (Figure 8-A-C). In the

Experiments and Modeling to Support Field Test Design

simulations with the weakest results ($\psi < \sim 0.5$), very weak dissolution is localized within the RoM pile near the vertical wall of the DRZ where brine enters the pile, with an accompanying minor decrease in porosity nearer the canister where evaporation of brine causes salt to precipitate (Figure 8-A). As ψ increases, the base of the RoM pile between the canister and the wall begins showing a stronger dissolution effect (Figure 8-B). A very slight decrease in porosity (< 0.01) appears above the canister, and an outer dissolution band develops in the margins of wall-side of the pile. Directly beneath the canister, porosity drops to its minimum value due to the evaporation of brine and precipitation of salt (Figure 8-C). These same regions of porosity change increase in magnitude and spatial extent as ψ increases further.

Finally, we present parameter sensitivity results for investigations of the initial saturation of the RoM pile (Figure 8-D), saturation of the DRZ (Figure 8-E), the relative strength of the maximum capillary pressure in the RoM salt compared to the DRZ (Figure 8-F), and simulations in which the DRZ is allowed to dry and depressurize for varying lengths of time (Figure 8-G). Each plot shows the porosity change severity index ψ as a function of the relevant variable. The index ψ scales approximately linearly with the initial saturation of the RoM salt and causes the greatest changes within the RoM pile. However, this porosity change is primarily expressed as a general decrease throughout the pile due to the precipitation of salt as water evaporates out of saturated brine. Sensitivity of ψ to the saturation of the DRZ is lower than RoM saturation until a critical threshold when it suddenly increases rapidly. For equally saturated RoM and DRZ salt, the relative maximum capillary strength of the RoM salt pile compared to the DRZ has little effect on ψ if capillary forces in the dry RoM pile are weak compared to the dry DRZ.

Based on the sensitivity to DRZ saturation, the elapsed time between opening of the drift and emplacement of the canister and ROM is likely to be important because the initially

Experiments and Modeling to Support Field Test Design

saturated walls of the DRZ drain towards the drift while losing water to evaporation. Our final sensitivity analysis investigates this topic (Figure 8-G) by adjusting the drainage time of the initial background simulations. Background simulations stabilize to a steady-state condition at about 60 days, as a steady pressure gradient from the far field boundary to the atmospheric boundary is established. As shown in Figure 8-G, effects of DRZ drainage and depressurization on the pile rapidly decrease after the first few days.

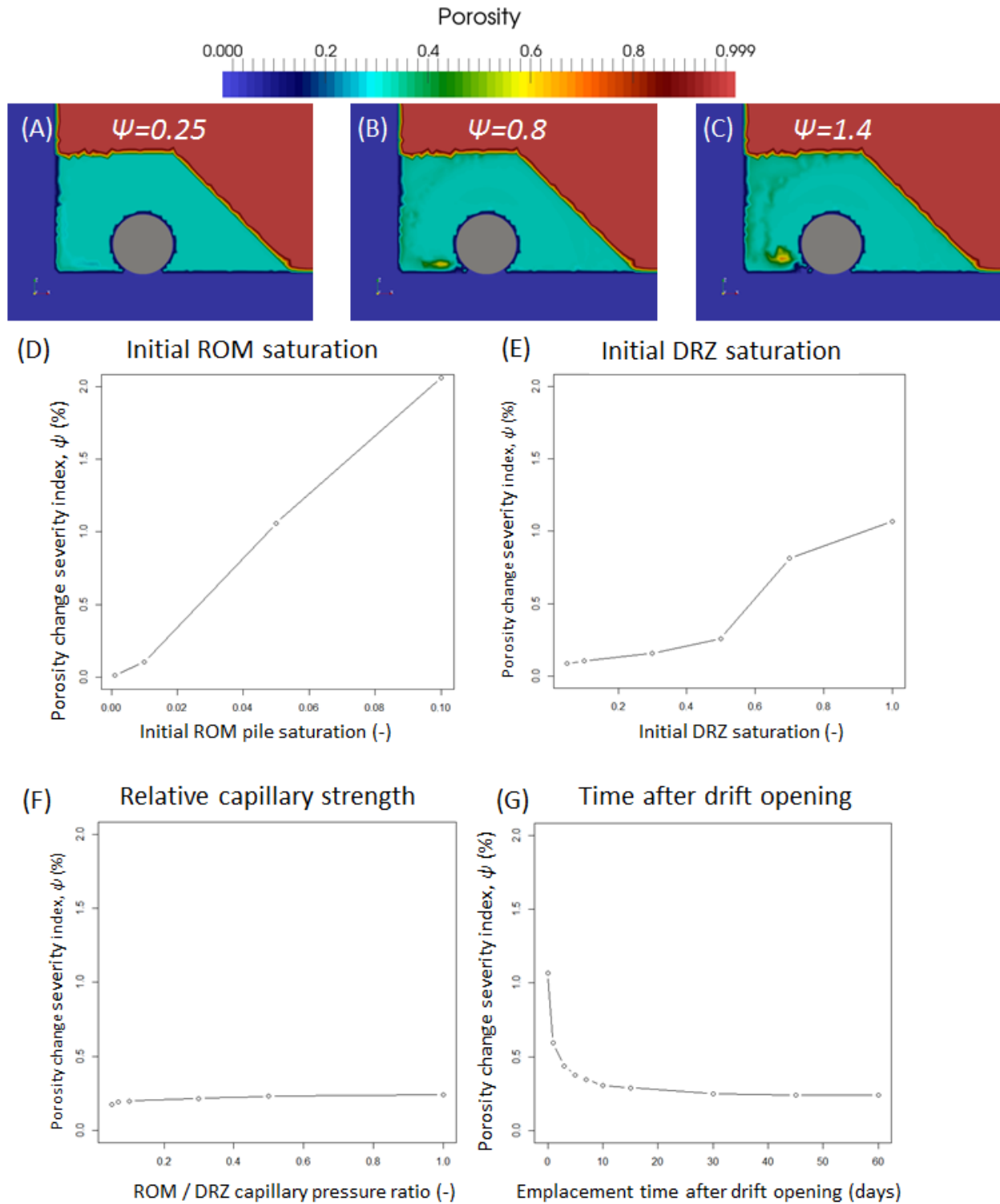


Figure 8: Sum of absolute value of porosity changes in pile (Ψ) resulting from different parameters. (A, B, and C) Example porosity effects with increasing Ψ . (D) RoM saturation; (E) Initial DRZ saturation; (F) Ratio of strength of maximum capillary effects in RoM salt vs. DRZ; (G) Elapsed time between opening of drift and placement of canister.

8. DISCUSSION AND CONCLUSION

We examine sensitivity of parameters (initial RoM saturation, DRZ saturation, RoM/DRZ capillary pressure ratio, and time between drift opening and waste placement) for their effect on the RoM salt pile dissolution and precipitation reactions. In contrast to previous work using retention functions that are not dependent on porosity, none of the simulations produce strong changes throughout the pile. Porosity changes are typically stronger near the wall of the drift and along the base of the RoM salt pile where entry of brine from the surrounding rock occurs. The parameter of greatest sensitivity is the initial saturation of the RoM salt pile, which at a saturation of 0.1 produced about double the porosity change compared to the fully saturated DRZ, as calculated using the porosity change severity index (ψ). However, the 0.1 saturation value for RoM salt may be unrealistically high in a generic salt repository setting because it requires an additional brine source following mining of the salt; assuming fully saturated salt at a porosity of 0.01, the initial porosity of the resulting RoM salt at a porosity of 0.3 would be about 0.03. Additional brine might enter RoM salt during the storage period between mining and emplacement of the canister from humid air or precipitation if RoM salt is stored outside, but the maximum reasonable value for these processes is unknown. Brine may also be generated in RoM salt by the dehydration of hydrous minerals during heating (Jordan et al., 2015c) or by the release of brine from fluid inclusions within the salt; however no evidence of this process has been seen in the current experiment.

Based on numerical simulations and experimental results during the first 100 days, little change is likely occurring in the RoM salt pile in the experiment. Temperature measurements indicate that thermal conductivity remains constant at a value typical for a porosity of 0.3, and no long-term trends are observed. If a strong dissolution band was forming, thermal conductivity

would be expected to decrease and further raise temperature. Conversely, if a portion of the pile was decreasing in porosity, local thermal conductivity would increase towards the $\sim 5.4 \text{ W/m}\cdot\text{K}$ typical of intact halite. Simulations show that porosity effects over time tend to be stronger in the RoM pile between the heated canister and the wall of the gallery. If this effect was in progress within the pile, temperature on the west (wall-side) and east (drift-side) of the pile should increasingly diverge from each other over time, but this is not observed. As is, the minor temperature variations after the initial heating period can likely be attributed to the cooling of ambient air due to the onset of winter, although a minor decrease in porosity and increase in thermal conductivity may account for the model overestimation of temperature in the top of the pile. More likely, however, the top of the pile is slightly more compacted than the sides of the pile and consequently has a lower porosity and correspondingly higher thermal conductivity. Tamping down of the pile to produce the flattened top could easily produce such a minor compaction increase.

In general, precipitation/dissolution appears to have little influence on the RoM pile in both the experiment and the simulations. Instead, a chimney effect and the flow of air through the drift combine to remove water vapor from the pile, reducing available brine, and preventing recharge of brine towards the heat source. Relatively cool air from the drift enters the pile and heats, increasing its air moisture holding capacity and desiccating the RoM salt. Warm, relatively dry air flows upward out of the pile and is entrained into the flow of ventilation air. The open chimney system causes a net drying of the RoM salt pile and restricts the cyclical dissolution/precipitation reactions that would be seen in a closed heat-pipe system (Olivella et al., 2011; Jordan et al., 2015a; Johnson et al., 2017a). Overall, this chimney effect is a contrast from prior experiments and simulations in closed systems, in which heat pipe effects produced

strong porosity changes (Jordan et al., 2015a,c; Johnson et al., 2017a; Olivella et al., 2011; Blanco-Martin et al., 2018). Additional changes within the RoM salt pile require a supply of brine, either from the DRZ or generated within the RoM salt pile by dehydration reactions.

Results for DRZ saturation and the ratio of maximum RoM to DRZ capillary pressure indicate that further porosity change can be induced in the pile by drawing water into the RoM salt pile from the wall and floor of the drift. However, this depends greatly on the quantity of water that is available in the DRZ. Since the DRZ capillary pressure at any given time depends on the saturation of the DRZ, there is a double sensitivity to DRZ saturation; increased DRZ saturation makes more brine available, and also reduces the capillary strength of the DRZ and allows increased wicking of brine into the RoM salt pile. The break in the DRZ saturation curve (Figure 8-E) indicates the point at which DRZ saturation lowers capillary pressure sufficiently to allow brine to enter the RoM salt pile.

Our work suggests several areas for further investigation. First, moisture content for run-of-mine salt from different locations and in different climates may be important. For WIPP RoM salt, moisture content tends to increase when relative humidity surpasses about 30% (Bourret et al., 2017). Furthermore, hydrous minerals within the RoM salt pile may dehydrate and contribute additional water (Jordan et al., 2015c). Minor fluid inclusions within individual salt clasts could also be released into the pile. Second, quantification of the brine available to the RoM pile from the surrounding walls needs to be improved. In addition to the initial porosity and permeability of the DRZ and intact wall rock, both of which can vary depending on local conditions, heating of the ambient salt drives reactions that release water. For typical WIPP salt, brine is released at temperatures between 60°C and 90°C (Johnson et al., 2017a), slightly warmer than the in-progress experiment but potentially achievable with a higher wattage heat source

and/or more canisters. With water liberated from hydrous minerals, additional brine could enter the RoM salt pile and amplify dissolution/precipitation effects around the heat source.

Experiments are currently in development to further examine brine generation in response to heat in the drift walls at WIPP (Johnson et al., 2017b). Finally, our simulations show that stronger porosity changes are likely to occur in a fresh drift than in an older drift. The ongoing experiment could not be conducted in a fresh drift due to facility requirements at the time of construction, but subsequent experiments in a new drift could help provide evidence to validate conceptual and numerical models.

9. ACKNOWLEDGEMENTS

This work was completed through collaboration between DOE-NE and DOE-EM. Funding and resources to engineer, develop, shakedown, and test a full-scale heater canister was initially provided in mid-FY 2013 through the DOE Carlsbad Field Office to LANL-Carlsbad Operations. This activity encompasses the work to operationally test a finished prototype heater at various heat outputs under in-situ conditions for use in future thermal tests in salt. As a collaborative effort, thermal and hydrological data collected for the operational test were used by Johnson to confirm model predictions with funding for the numerical analysis provided by DOE-NE through grant DMS SFWD-SFWST-2017-000102.

10. REFERENCES

- Bechtold, W., E. Smailos, S. Heusermann W. Bollingerfehr, B. Bzaragan Sabet, T. Rothfuchs, P. Kamlot, J. Grupa, S. Olivella, and Hansen, F.D. 2004. Backfilling and sealing for underground repositories for radioactive waste in salt (BAMBUS II project). Final Report EUR 20621. Nuclear Science and Technology, Luxembourg.
- Birkholzer, J.T. 2004. Estimating liquid fluxes in thermally perturbed fractured rock using measured temperature profiles. *Journal of Hydrology*, 327(3-4), 496-515. doi:10.1016/j.jhydrol.2005.11.049.
- Blanco-Martín, L., J. Rutqvist, A. Battistelli, and J.T. Birkholzer. 2018. Coupled processes modeling in rock salt and crushed salt including halite solubility constraints: Application to disposal of heat-generating nuclear waste. *Transport in Porous Media* 124(1), 159-182. <https://doi.org/10.1007/s11242-018-1057-7>
- Bourret, S.M., P.J. Johnson, G.A. Zyvoloski, S.P. Chu, D.J. Weaver, S. Otto, H. Boukhalfa, F.A. Caporuscio, A.B. Jordan, and P.H. Stauffer. 2016. Experiments and modeling in support of generic salt repository science. Los Alamos National Laboratory, USDOE Used Fuel Disposition Campaign, Final Report LA-UR-16-27329
- Bourret, S.M., S. Otto, P.J. Johnson, D.J. Weaver, H. Boukhalfa, and P.H. Stauffer. 2017. High level waste in salt repositories: Experiments and simulations of evaporation in the underground. *Waste Management 2017 Proceedings*.
- Brewitz, W. and T. Rothfuchs. 2007. Concepts and Technologies for Radioactive Waste Disposal in Rock Salt. *Acta Montanistica Slovaca Ročník* 12(1), 67–74.
- Callahan, G., D.C. Guerin, D.G. Levitt, D.L. Newell, B.A. Robinson, and L. Van Sambeek. 2012. Salt Repository Synthesis Data of Non-Delaware Basin and International Programs for the Storage/Disposal of Nuclear Waste. Los Alamos National Laboratory Report LCO-SDI-002.
- Caporuscio, F.A., H. Boukhalfa, M.C. Cheshire, A.B. Jordan, and M. Ding. 2013. Brine migration experimental studies for salt repositories. FCRD Used Fuel Disposition Campaign Milestone FCRD-UFD-2013-000204.
- Carter, J.T., F. Hansen, R. Kehrman, and T. Hayes. 2011. A generic salt repository for disposal of waste from a spent nuclear fuel recycle facility. SRNL-RP-2011-00149 Rev. 0. Savannah River National Laboratory.
- Cinar, Y., G. Pusch, and V. Reitenbach. 2006. Petrophysical and capillary properties of compacted salt. *Transport in Porous Media* 65(2), 199-228.
- DOE Carlsbad Field Office (DOE CBFO). 2012. A Management Proposal for Salt Defense Disposal Investigations (SDDI) for the Disposal of DOE-EM Managed Wastes. U.S. Department of Energy Carlsbad Field Office document.
- Faghri, A. 1995. Heat pipe science and technology. Taylor and Francis Group, Boca Raton, Florida.
- Fahland, S. and S. Heusermann. 2013. Geomechanical analysis of the integrity of waste disposal areas in the Morsleben repository. *Rock Characterisation, Modelling, and Engineering Design Methods*, Taylor & Francis Group, London, ISBN 978-1-138-00057-5.

Experiments and Modeling to Support Field Test Design

- Gable, C.W.; Clayton, D.J.; Lu, Z. 2009. Inverse modeling to determine thermal properties of salt due to heating from high level waste emplaced in a generic salt repository. US DOE Office of Nuclear Fuel Recycling Report AFCI-WAST-PMO-DV-2009-000001.
- Haar, L., J.S. Gallagher, and G.S. Kell. 1984. NBS/NRC Steam, Tables. Hemisphere, New York.
- Hansen, F.D. and C.D. Leigh. 2011. Salt disposal of heat-generating nuclear waste. Sandia National Laboratories Report SAND2011-0161.
- Hansen, F.D.M., W. Steininger, and W. Bollingerfehr. 2017. Proceedings of the 7th US/German Workshop on Salt Repository Research, Design, and Operation. Sandia National Laboratories, SFWD-SFWST-2017-000008, SAND2017-1057R
- Harp, D.R., P.H. Stauffer, P.K. Mishra, D.G. Levitt, and B.A. Robinson. 2014. Modeling of high-level nuclear waste disposal in a salt repository. Nuclear Technology 187:294-307. Doi:10.13182/NT13-110
- Hess, H.H., J.N. Adkins, W.B. Heroy, W.E. Benson, M.K. Hubbert, J.C. Frye, R.J. Russell, and C.V. Theis. 1957. The disposal of radioactive waste on land, report of the committee on waste disposal of the division of earth sciences. Publication 519, National Academy of Sciences - National Research Council.
- Ho, C. and S. Webb. 1998 Review of porous media enhanced vapor-phase diffusion mechanisms, models, and data: Does enhanced vapor-phase diffusion exist? J. Porous Media 1:71-92.
- Johnson, P.J., S.M. Bourret, H. Boukhalfa, F.A. Caporuscio, G.A. Zyvoloski, D.J. Weaver, S. Otto, and P.H. Stauffer. 2017. Experiments and Modeling to Support Field Test Design. Los Alamos National Laboratory, SFWD-SFWST-2017-000102, LA-UR-17-27759, Los Alamos, NM.
- Johnson, P.J., H. Boukhalfa, D.J. Weaver, S. Otto, B.L. Dozier, P.H. Stauffer, M.M. Mills, E.N. Matteo, K.L. Kuhlman, J. Rutqvist, and Y. Wu. 2017. Test plan document for thermal testing in salt. US Dept. of Energy Used Fuel Disposition Campaign, DOE Milestone M3SF-18LA010303013.
- Johnson, P.J., G.A. Zyvoloski, and P.H. Stauffer. In Review. Impact of a porosity-dependent retention function on simulations of porous flow. Transport in Porous Media.
- Jordan, A.B., H. Boukhalfa, F.A. Caporuscio, and P.H. Stauffer. 2015. Brine Transport Experiments in Run-of-Mine Salt. Los Alamos National Laboratory Report LA-UR-15-26804. Los Alamos, NM.
- Jordan, A.B., G.A. Zyvoloski, D.J. Weaver, S. Otto, and P.H. Stauffer. 2015. Coupled Thermal-Hydrologic-Chemical Model for In-Drift Disposal Test. Los Alamos National Laboratory Report LA-UR-15-27442. Los Alamos, NM.
- Jordan, A.B., H. Boukhalfa, F.A. Caporuscio, B.A. Robinson, and P.H. Stauffer. 2015. Hydrous Mineral Dehydration around Heat-Generating Nuclear Waste in Bedded Salt Formations. *Environmental Science & Technology*, 5, 1-13. DOI: 10.1021/acs.est.5b01002.


- Krieg, R.D. 1984. Reference stratigraphy and rock properties for the Waste Isolation Pilot Plant (WIPP) project. Sandia National Laboratories Report SAND-83-1908.
- Kuhlman, K.L and B. Malama. 2013. Brine flow in heated geologic salt. Sandia National Laboratories Report SAND2013-1944. Albuquerque, NM.
- Lappin, A.R. 1988. Summary of site-characterization studies conducted from 1983 through 1987 at the Waste Isolation Pilot Plant (WIPP) site, southeastern New Mexico. In: Post, R.G., High-level waste and general interest: Volume II, p.371-376. Waste Management: Symposium on Radioactive Waste Management, Tucson, AZ, 28 Feb – 3 Mar.
- McTigue, D.F., and E.J. Nowak. 1987. Brine transport studies in the bedded salt of the Waste Isolation Pilot Plant (WIPP). Sandia National Labs report SAND-87-1274C.
- Millington, R.J. and J.P. Quirk. 1961. Permeability of porous solids. Transactions of the Faraday Society 57:1200-1207. Doi:10.1039/TF9615701200
- Munson, D.E., R.L. Jones, J.R. Ball, R.M. Clancy, D.L. Hoag, and S.V. Petney. 1990. Overtest for simulated defense high-level waste (Room B): In situ data report (May 1984-February 1988): Waste Isolation Pilot Plant (WIPP) Thermal/Structural Interactions Program. Sandia National Labs Technical Report SAND-89-2671.
- Olivella, S., S. Castagna, E.E. Alonso, and A. Lloret. 2011. Porosity variations in saline media induced by temperature gradients: experimental evidences and modeling. Transport in porous media, 90(3), 763-777.
- Powers, D.W., S.J. Lambert, S. Shaffer, L.R. Hill, and W.D. Weart, ed. 1978. Geological characterization report, Waste Isolation Pilot Plant (WIPP) site, southeastern New Mexico. Waste Management Technology, Sandia Laboratories, Albuquerque, New Mexico.
- Pruess, K. 1991. TOUGH2—A general-purpose numerical simulator for multiphase fluid and heat flow. Lawrence Berkeley Laboratory LBL-29400.
- Recherd, R.P. 2000. Historical background on performance assessment for the Waste Isolation Pilot Plant. Reliability Engineering & System Safety 69(1-3), 5-46.
[https://doi.org/10.1016/S0951-8320\(00\)00023-5](https://doi.org/10.1016/S0951-8320(00)00023-5)
- Robinson, B.A., N.Z. Elkins, and J.T. Carter. 2012. Development of a U.S. Nuclear Waste Repository Research Program in Salt. Nuclear Technology. 180(1), 122-138. DOI: 10.13182/NT12-A14524
- Rutqvist, J., L.B. Martin, S. Molins, D. Trebotich, and J. Birkholzer, 2016. Modeling coupled THM processes and brine migration in salt at high temperatures. Lawrence Berkeley National Laboratory, UFD Document FCRD-UFD-2015-000366, LBNL-191216.
- Sparrow, B.S. 2003 Empirical equations for the thermodynamic properties of aqueous sodium chloride. Desalination 159(2):161-170. [https://doi.org/10.1016/S0011-9164\(03\)90068-3](https://doi.org/10.1016/S0011-9164(03)90068-3)
- Stauffer, P.H., J.A. Vrugt, H.J. Turin, C.W. Gable, and W.E. Soll. 2009. Untangling diffusion from advection in unsaturated porous media: Experimental data, modeling, and parameter uncertainty. Vadose Zone Journal 8(2):510-522. Doi:10.2136/vzj2008.0055.

Experiments and Modeling to Support Field Test Design

- Stauffer, P.H., D.R. Harp, A.B. Jordan, Z. Lu, S. Kelkar, Q. Kang, J. Ten Cate, H. Boukhalfa, Y. Labayed, P.W. Reimus, F.A. Caporuscio, T.A. Miller, and B.A. Robinson. 2013. Coupled model for heat and water transport in a high level waste repository in salt. Los Alamos National Laboratory Document, LA-UR-13-27584.
- Stauffer, P.H., K.C. Lewis, J.S. Stein, B.J. Travis, P. Lichtner, and G.A. Zyvoloski. 2014 Joule-Thomson effects on the flow of liquid water. *Transport in Porous Media* 105(3), DOI 10.1007/s11242-014-0379-3
- Stauffer, P.H., A.B. Jordan, D.J. Weaver, F.A. Caporuscio, J.A. Ten Cate, H. Boukhalfa, B.A. Robinson, D.C. Sassani, K.L. Kuhlman, E.L. Hardin, S.D. Sevougian, R.J. MacKinnon, Y. Wu, T.A. Daley, B.M. Freifield, P.J. Cook, J. Rutqvist, and J.T. Birkholzer. 2015. Test Proposal Document for Phased Field Testing in Salt. US DOE-NE Used Fuel Disposition Campaign, Level 2 Milestone M2FT-15LA08119016, FCRD-UFD-2015-000077, Los Alamos National Laboratory Document LA-UR-15-23154.
- Stoller Inc. 2014. Independent design analysis and verification of “heater canister” as part of the Salt Defense Disposal Investigation. Comprehensive Final Report.
- Tsang, C.F., F. Bernier, and C. Davies. 2005. Geohydromechanical processes in the excavation damage zone in crystalline rock, rock salt, and indurated plastic clays – in the context of radioactive waste disposal. *Int J Rock Mech and Mining Sci.* 42(1):109-125.
- Washington Savannah River Company, Washington Safety Management Solutions, Sandia National Laboratories, Los Alamos National Laboratory. 2008. A Generic Salt Repository for Disposal of Waste from a Spent Nuclear Fuel Recycling Facility. Predecisional Draft, Rev 1 (September). GNEP-WASTMTSD-MI-RT-2008-000245. Aiken, SC: U.S. Department of Energy.
- Wollrath, J., R. Mauke, M. Mohlfeld, M. Niemeyer, and D.A. Becker. 2014. Morsleben repository – Interdependence of technical feasibility and functionality of geotechnical barriers and safety case development. *Radioactive Waste Management NEA/RWM/R(2013)9*
- Zyvoloski, G.A., B.A. Robinson, Z.V. Dash, S. Kelkar, H.S. Viswanathan, R.J. Pawar, P.H. Stauffer, T.A. Miller, and S.P. Chu. 2012. Software users manual (UM) for the FEHM Application Version 3.1-3.X. LANL Report, LA-UR-12-24493

APPENDIX A: SLIDES FOR INTERPORE PRESENTATION

The following slides were presented at InterPore 2018 as part of a session on advances in numerical modeling. A generalized model function (Johnson et al. in review) is presented for handling capillary effects in salt domains where porosity changes.


**U.S. DEPARTMENT OF
ENERGY**

Nuclear Energy

LA-UR-18-23570

**A Numerical Modeling Approach for Capillary
Effects in Systems with Changing Porosity**

Peter Johnson, George Zyvoloski, Phil Stauffer
May 23, 2017

**Los Alamos**
NATIONAL LABORATORY
EST. 1943

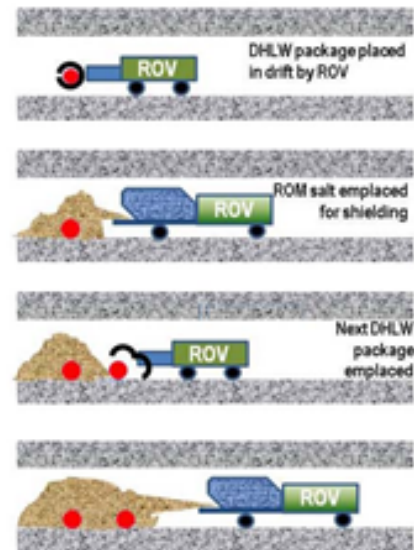
Interpore 2018, New Orleans, LA



LA-UR-18-23570

Background: Hot Nuclear Waste in salt

- **Motivation: in-drift disposal of heat-generating nuclear waste (HGNW) in salt**
- **Focus on ROM salt surrounding HGNW canister**
- **Potential for porosity changes in salt**



Carter, J.T., F. Hansen, R. Kehrman, and T. Hayes 2011b. A generic salt repository for disposal of waste from a spent nuclear fuel recycle facility. SRNL-RP-2011-00149 Rev. 0. Savannah River National Laboratory.



LA-UR-18-23570

General problem

■ **Model retention functions are commonly assigned at start of model run**


- $P_c = f(S_l)$ Saturation-only retention function

■ **If porosity changes, function becomes inaccurate**

■ **Can stop model run, set new function, start again**

- Inefficient
- Requires user to decide when to change functions
- Can be difficult when porosity changes are spatially unpredictable

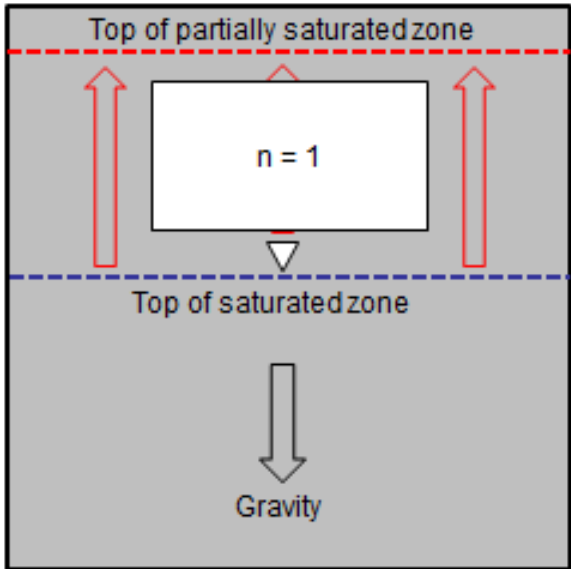
■ **Objective: Make a function that dynamically calculates $P_c = f(n, S_l)$**



U.S. DEPARTMENT OF
ENERGY
Nuclear Energy


LA-UR-18-23570

Model retention functions: A thought experiment



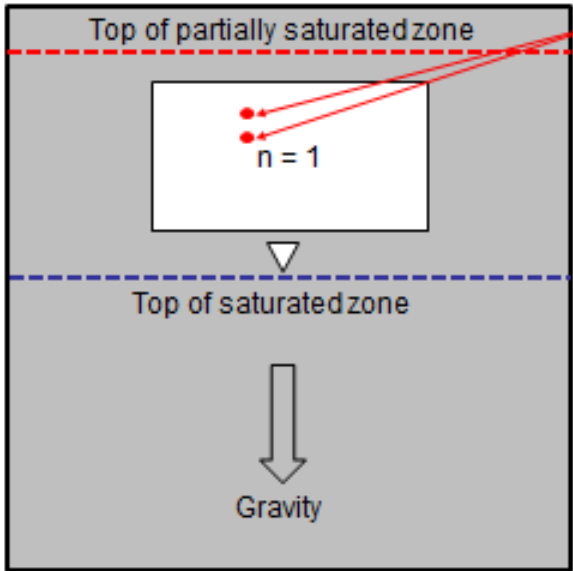
- Consider a simple homogeneous, isotropic porous medium which is partially filled with water
- Appropriate capillary effects measured, applied as retention function in model
 - Upward draw of water beyond capillary fringe leads to a zone of partial saturation: equal saturation at any given height above base of box
- Then a portion of the box becomes completely porous ($n = 1$)
 - Retention function remains as at start of run, with capillary pressure as function of saturation

4



LA-UR-18-23570

Retention function: Problems



- Nodes: porosity = 1, saturation < 1 for both
- Vertically stacked, open air nodes are both partially saturated
- Implies an unphysical retention of water in air
 - Gravity should drain upper nodes into lower nodes, but capillary function prevents that
- *There should be no capillary effect in this void space*

5



LA-UR-18-23570

Revised function

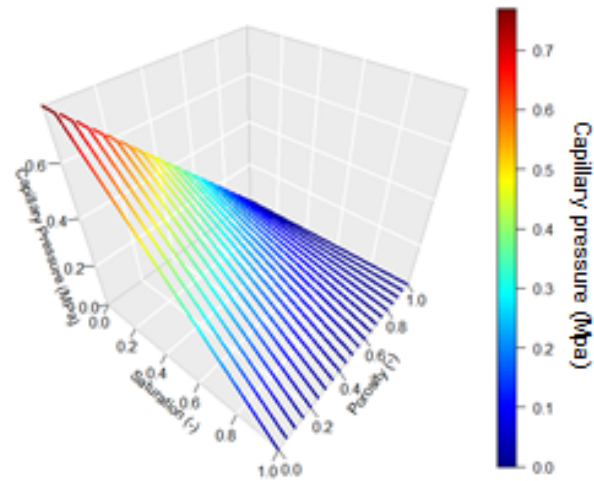
- Residual saturation and maximum capillary pressure updated in each timestep

$$S_r(n) = S_{ri} \frac{1-n}{1-n_i}$$

- Subscript i is initial value specified by user

$$P_{cmax} = P_{cmaxi} \left(\frac{1-n}{1-n_i} \right)$$

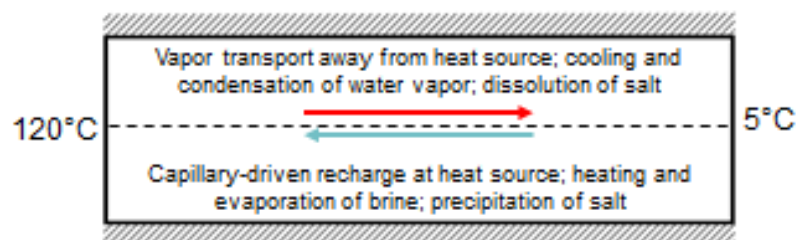
- Then linear function $P_c = f(S_l)$ applied to updated endpoints





LA-UR-18-23570

Example: Simple salt cylinder



Model domain based on experiments by Olivella et al. (2011)

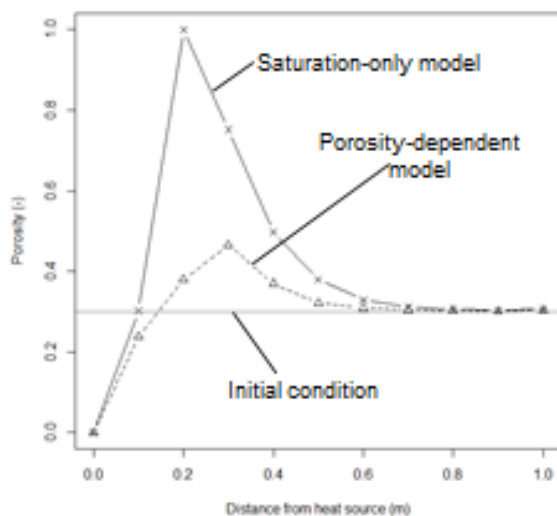
Evaluating porosity, saturation, and volumetric water content through center of cylinder

Olivella, S., Castagna, S., Alonso, C.E., and Lloret, J. (2011) Porosity variations in saline media induced by temperature gradients: experimental evidences and modeling. *Transport in porous media*, 90(3): 769-777.



LA-UR-18-23570

Results: Porosity

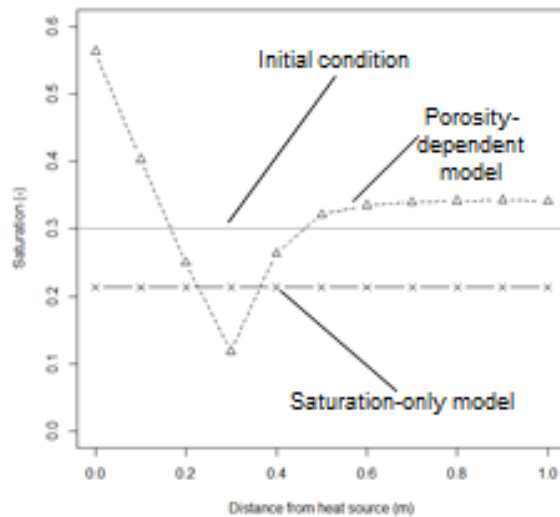


- Saturation-only model shows total dissolution at 20 cm
- Porosity-dependent model increases distance of maximum dissolution and reduces severity
- Both models show limited dissolution in cooler regions, and strong precipitation effect near heat source



LA-UR-18-23570

Results: Saturation



■ **Saturation-only model balances saturation equally throughout domain**

■ **Porosity-dependent model is highly variable**

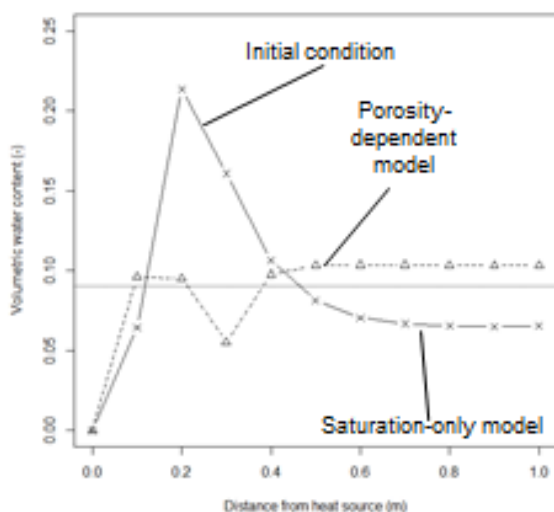
- Reduced saturation of higher-porosity regions, increased in lower-porosity regions



LA-UR-18-23570

Results: Volumetric water content

■ $VWC = \text{porosity} \times \text{saturation}$

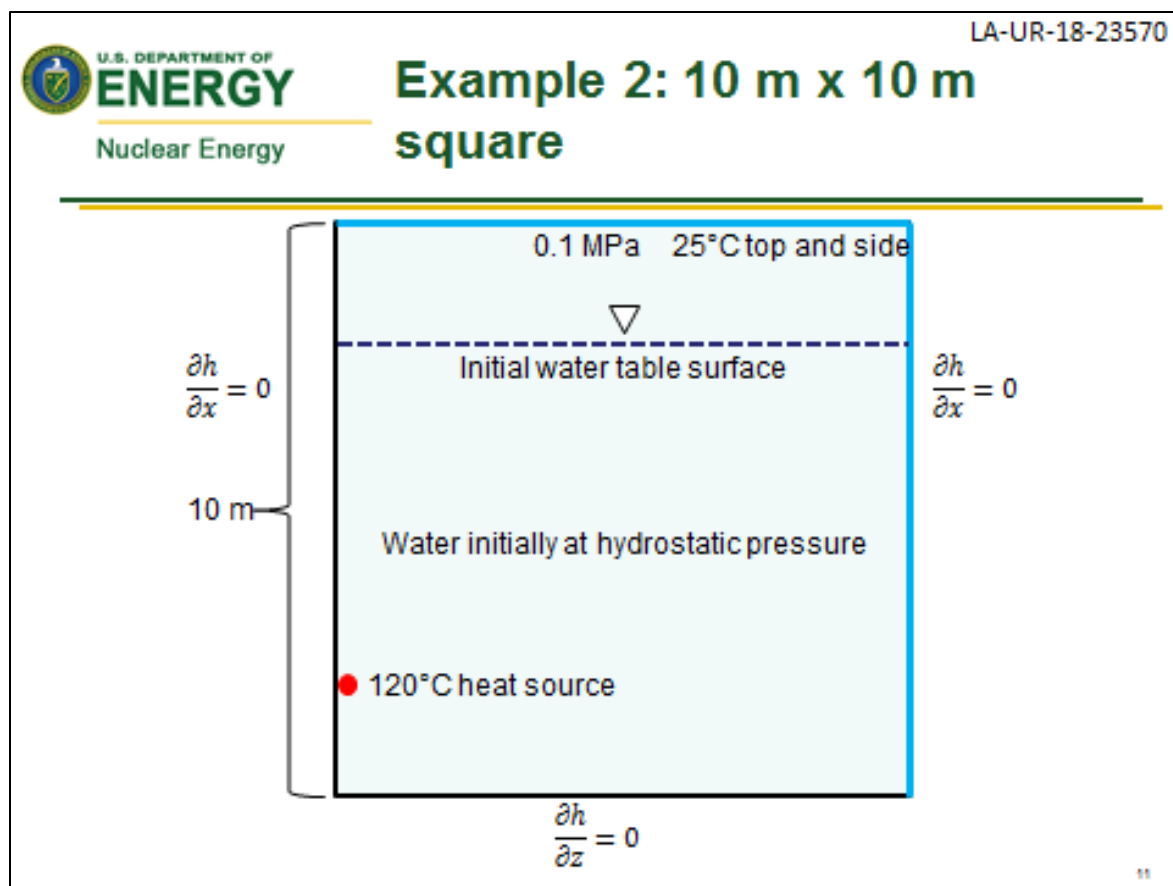


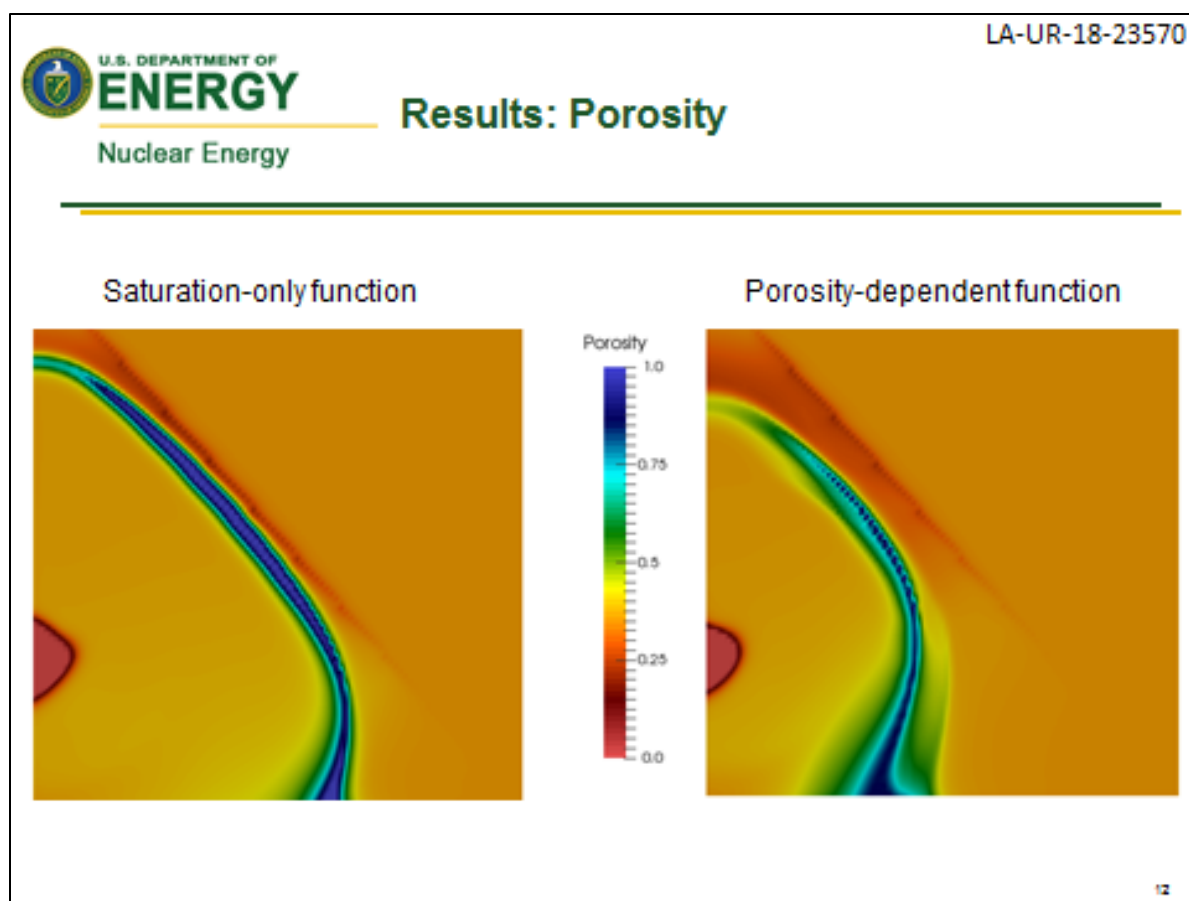
■ **Saturation-only model**
balances saturation evenly
throughout domain

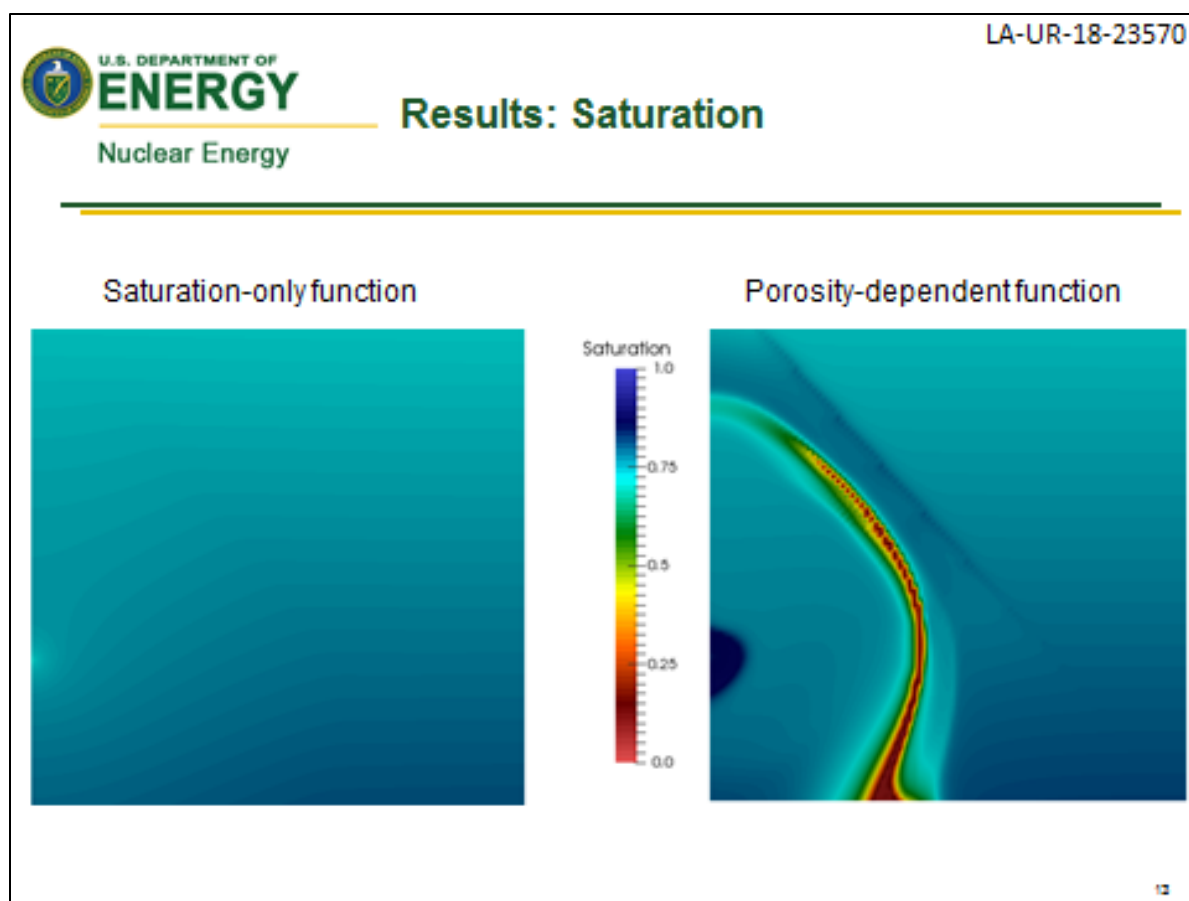
- Volumetric water content directly follows porosity

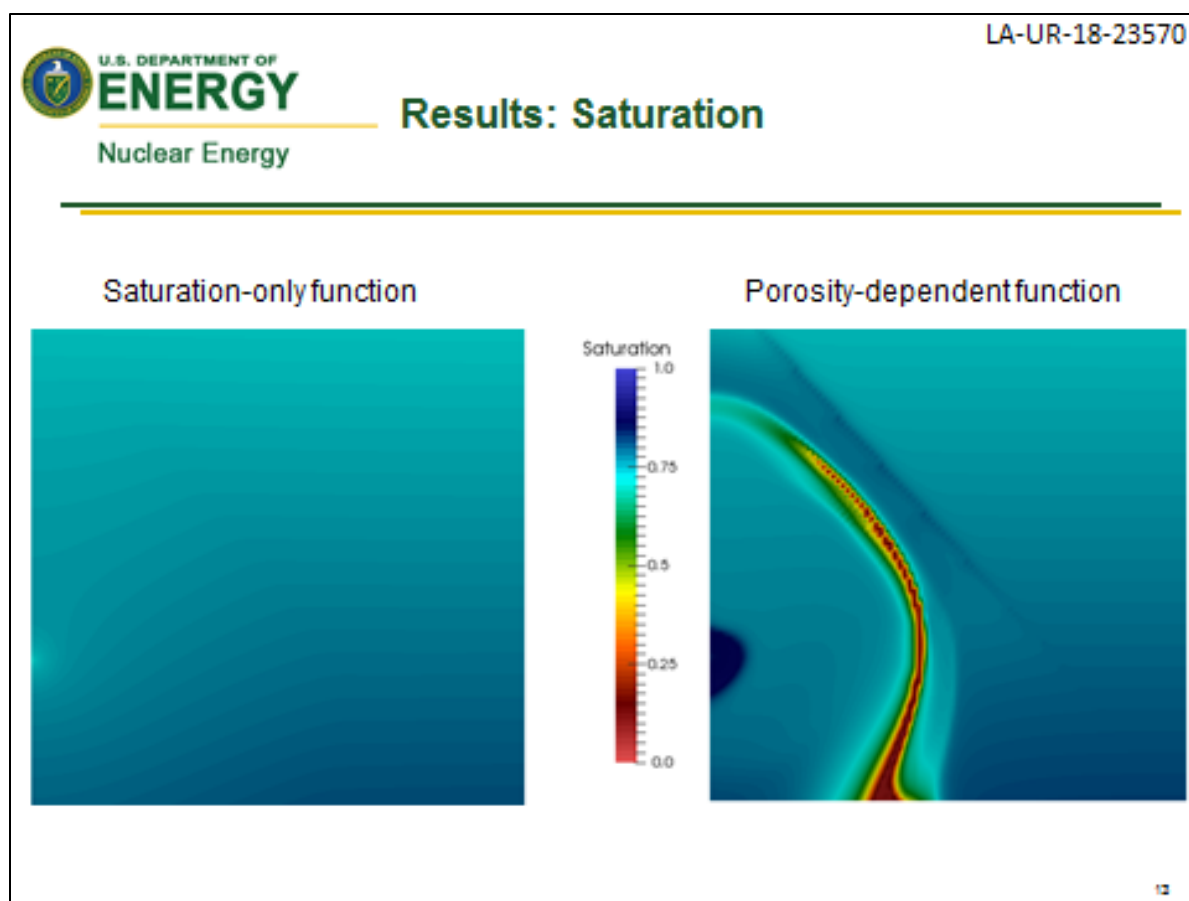
■ **Porosity-dependent model**
preferentially dries
dissolution zone

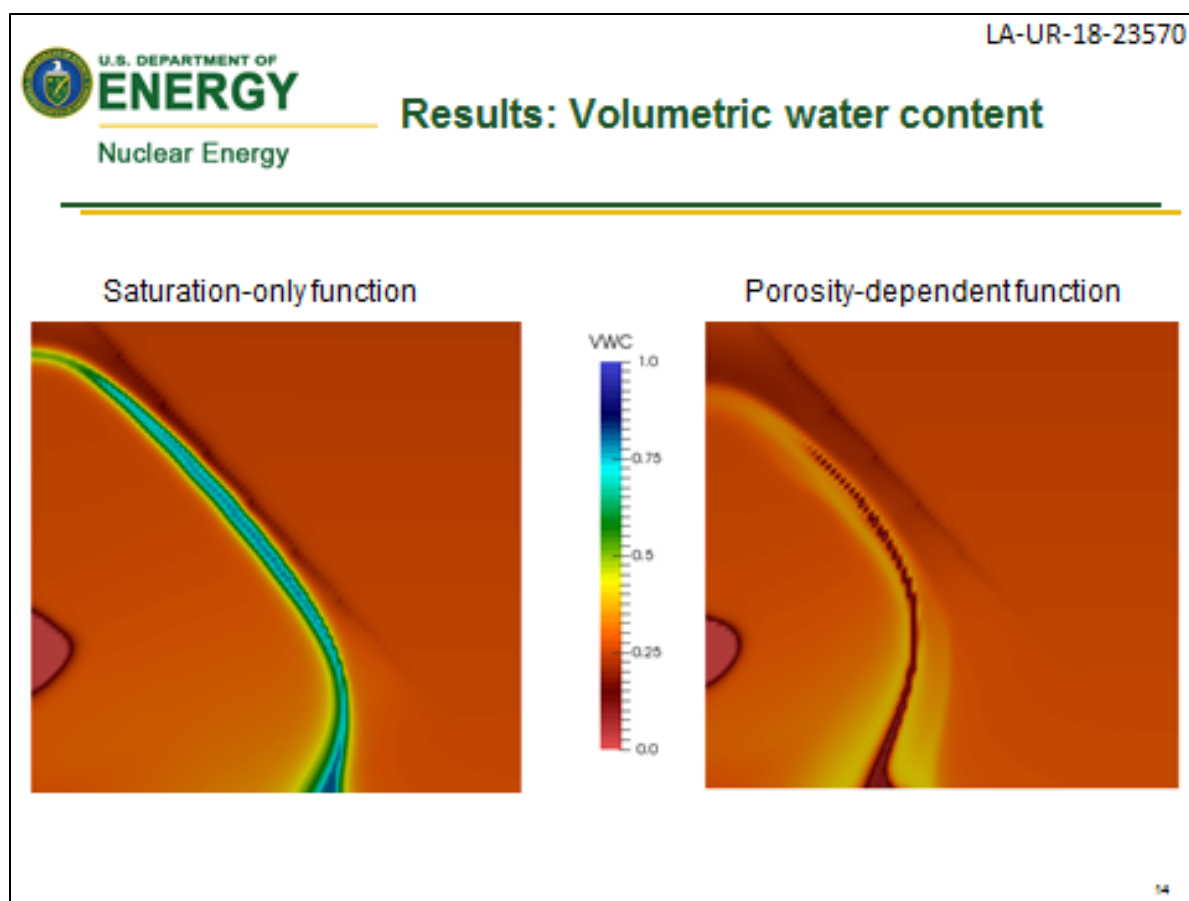
■ ***Inversion of volumetric water content results***














LA-UR-18-23570

Conclusions

■ Porosity-dependent retention function strongly alters model results

- Fixes clearly unphysical problems at high porosity
 - Eliminates issues with water retention in porosity=1 regions
 - Avoids issues with equal saturation independent of material properties
- Alters magnitude and location of porosity changes in capillary-driven systems
- Inverts volumetric water content results compared to fixed, saturation-only function



U.S. DEPARTMENT OF
ENERGY
Nuclear Energy

LA-UR-18-23570

Acknowledgements

■ This work was funded by the DOE Office of Nuclear Energy,
grant DMS SFWD-SFWST-2017-000102

18

APPENDIX B: ADDITIONAL EXPERIMENT INFORMATION

The following material is supplemental information about the ongoing canister heater experiment.

ROM experiment schematics and images

Early scoping efforts planned for an experiment with five canisters in a newly mined drift. An unrelated accident at WIPP in 2014 resulted in the cessation of mining activities throughout the facility and necessitated an adjustment of the experiment design. A smaller scale field test was therefore proposed with a single heater in ROM salt. Due to restricted ventilation in WIPP, the experiment site was relocated to near a ventilation shaft at WIPP, in a wide tunnel which has been open since the early days of the facility. Based on facility access requirements, a schematic was developed (Figure 9) with the ROM salt pile abutted against the wall of the facility with a downward slope. Based on this schematic, the numerical meshes for FEHM were developed.

During the construction of the experiment, the downward-sloping pile top near the drift wall proved difficult to precisely construct, so the decision was taken to fill in that wedge and flatten the top of the pile (Figure 10). The same numerical mesh was applied, but with a redefinition of the nodes in the affected area to RoM salt properties instead of air.

END VIEW OF CANISTER UNDER ROM SALT

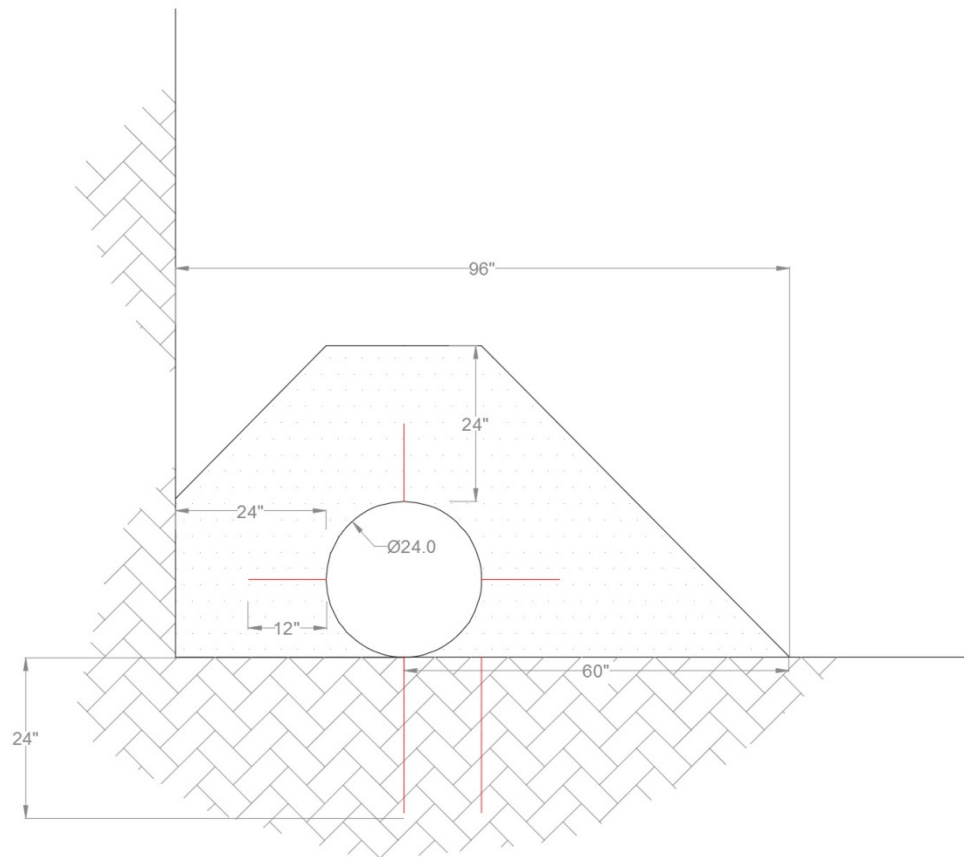


Figure 9: Initial schematic of experiment setup. Circle in center is canister. Red lines indicate thermocouple arrays for temperature. Numbers are dimensions in inches.

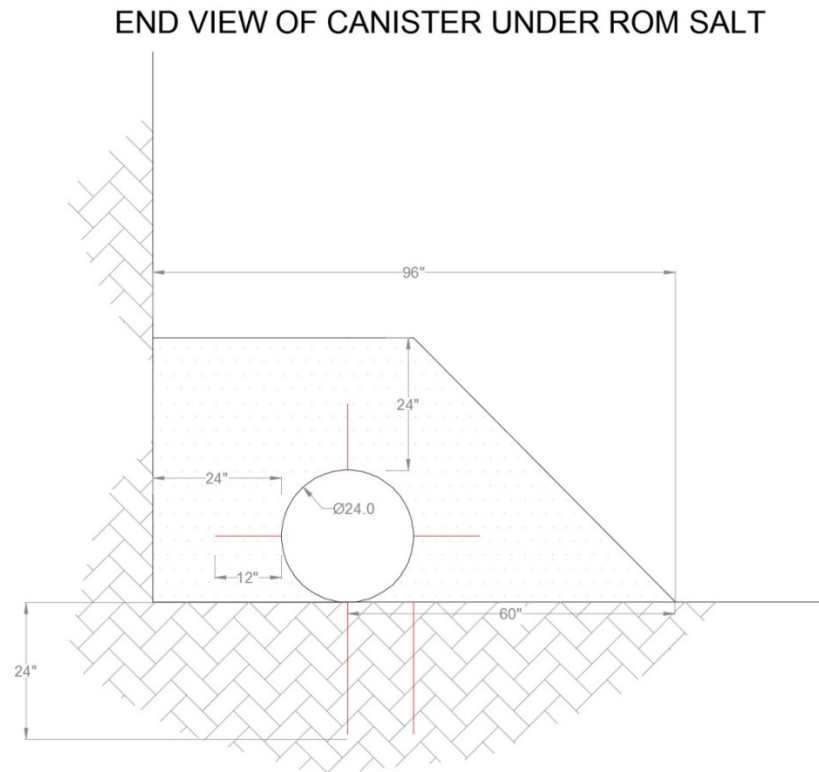
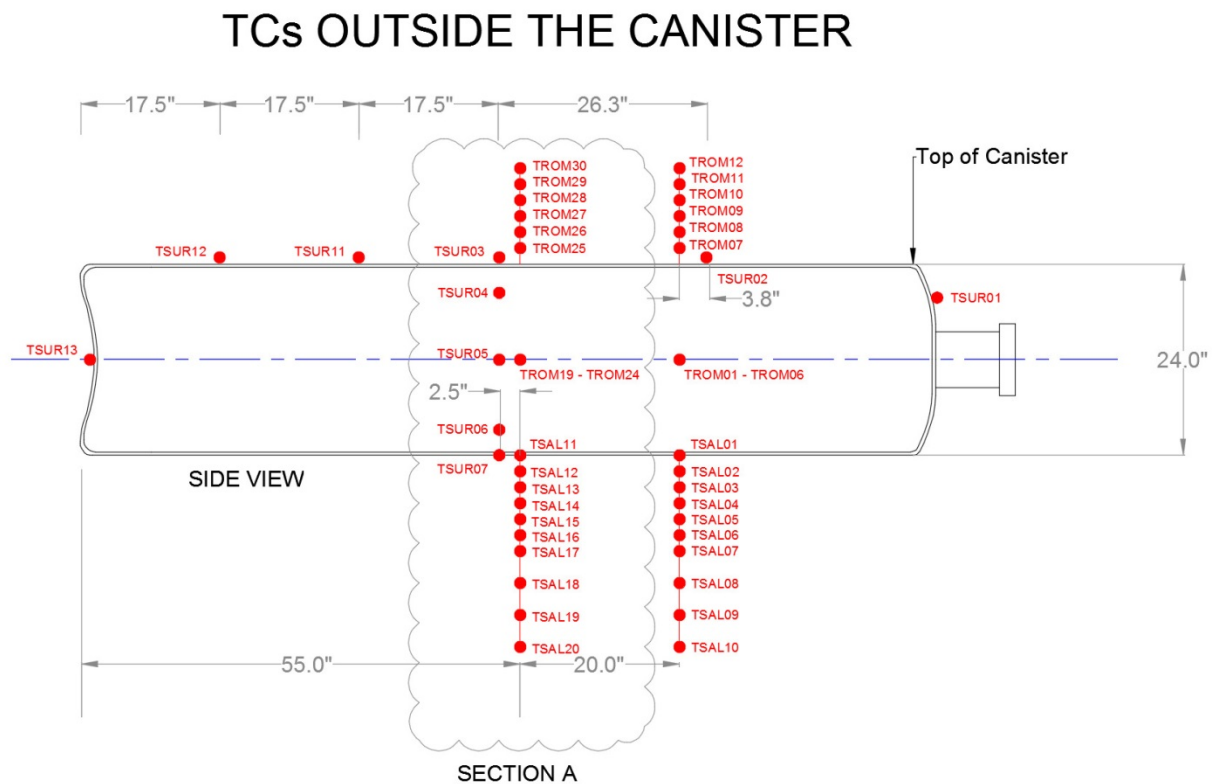


Figure 10: End view of revised schematic, similar to initial schematic but with flattened top of pile extended to wall (top), and constructed ROM salt pile (bottom).

Instrument locations

Thermocouple arrays are placed in transects around the canister (Figure 11). Two main arrays are employed laterally to the canister, with additional measurements at points along the canister exterior. For the 2-D modeling employed in this manuscript the array in the canister center is used for comparison (Figure 12). Arrays were placed in the floor of the facility by drilling a small (2.54 cm diameter) borehole, pressing the thermocouple array against the borehole wall, and then



All dimensions in inches

THEA = Thermocouples on the heater strips inside the canister (1-5)

TSUR = Thermocouples on the surface of the canister (1-13)

TROM = Thermocouples in the ROM salt above and to the sides of the canister (1-36)

TSAL = Thermocouples in the intact salt underneath the canister (1-30)

Figure 11: ROM arrays (red) around canister. Numbers indicate designation for thermocouples as shown in Figures 12 and 13-17.

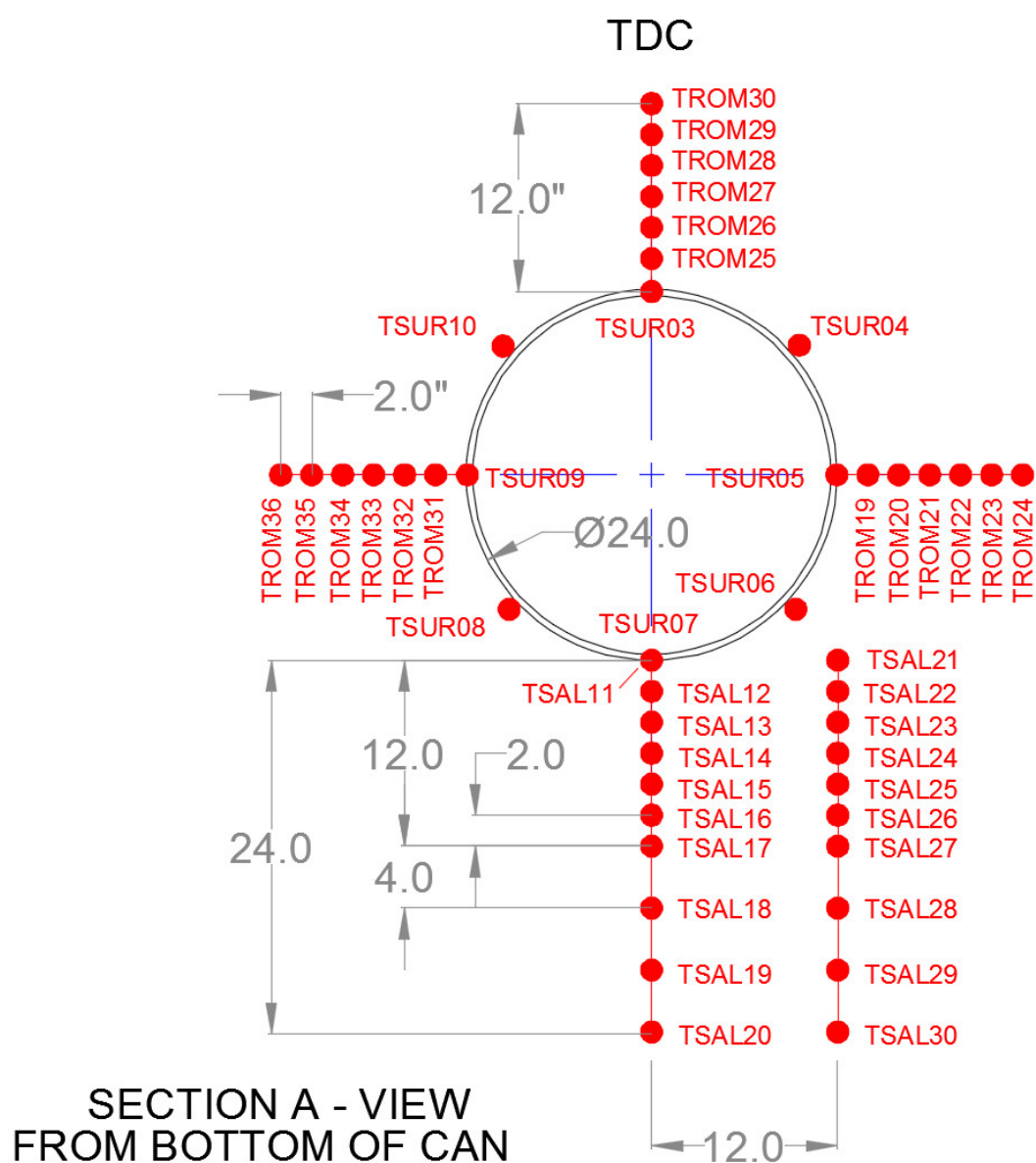


Figure 12: Thermocouple arrays with designators for subsequent data. TROM indicates arrays placed in ROM salt pile; TSAL arrays are placed in the intact salt of the floor; and TSUR are on the surface of the canister.

Temperature data from instruments

Temperatures are measured by thermocouples and recorded at a central datalogger every 15 minutes. The following plots (Figures 13-16) show measured temperatures on the thermocouple arrays above, lateral to (west and east, with west oriented towards the wall of the drift), and below the canister respectively. Points on all plots correspond with measurement locations in Figure 12. In all cases, temperature stabilized at approximately 15 days, excluding a brief power outage. A long-term slight decrease in temperature has been observed, likely because cooler winter air has been passed into WIPP. Daily fluctuations and storm events induce temperature changes of up to a few degrees in the pile.

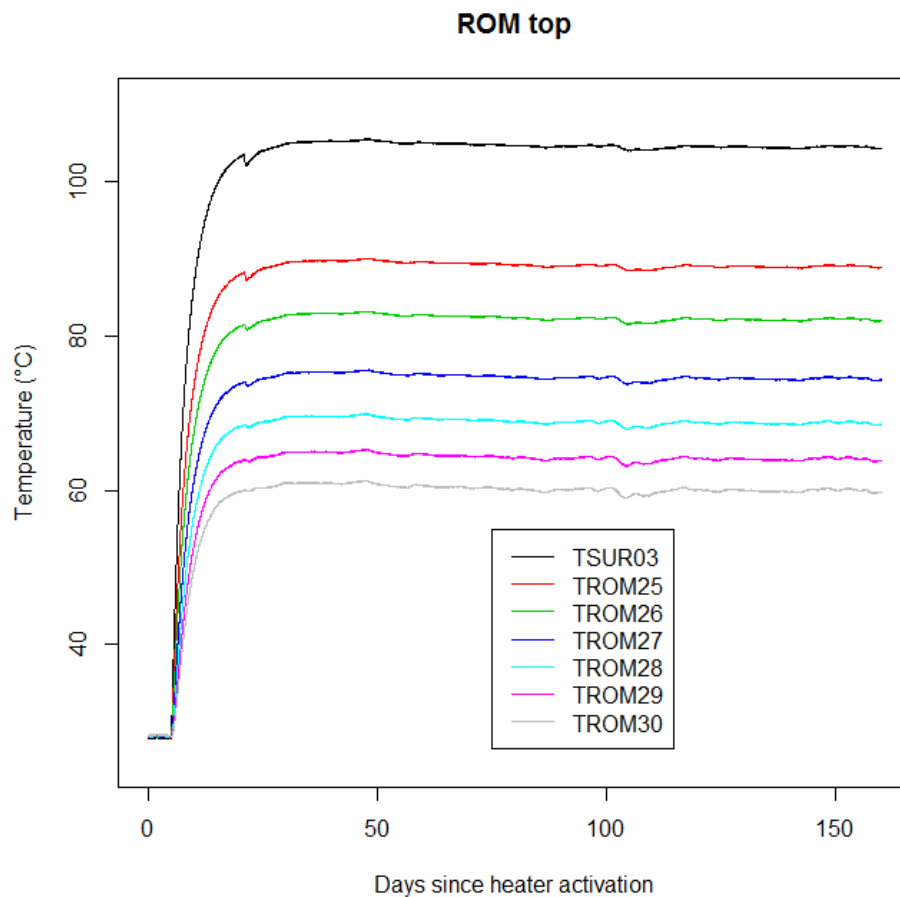


Figure 13: Temperature measurements for transect extending vertically upward from canister. Thermocouple labels are shown as in Figure 12.

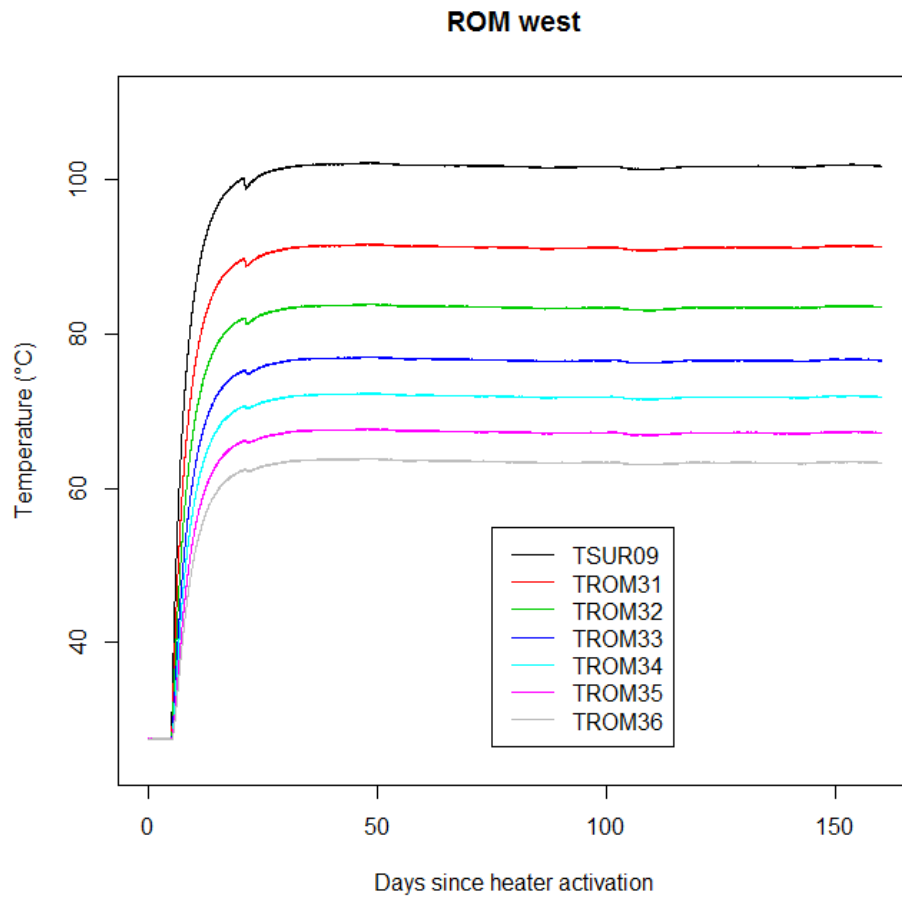


Figure 14: Temperature measurements for transect extending laterally west (left in Figures 10 and 12) from canister. Thermocouple labels are shown as in Figure 12.

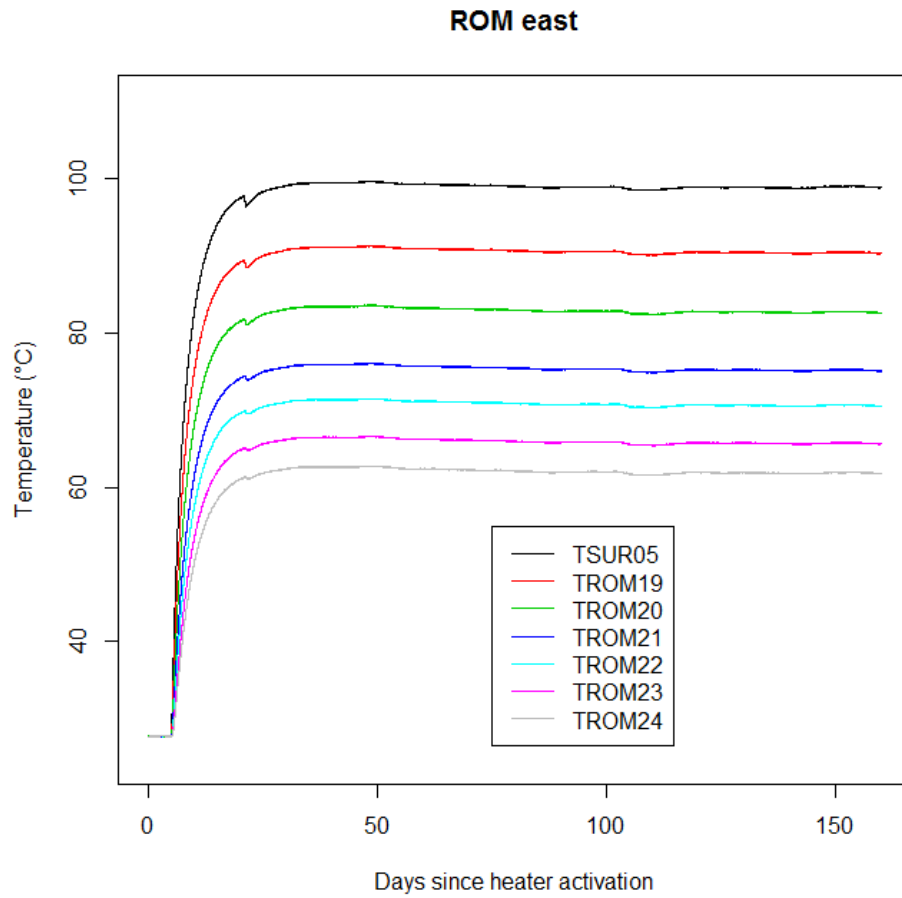


Figure 15: Temperature measurements for transect extending laterally east (right in Figures 10 and 12) from canister. Thermocouple labels are shown as in Figure 12.

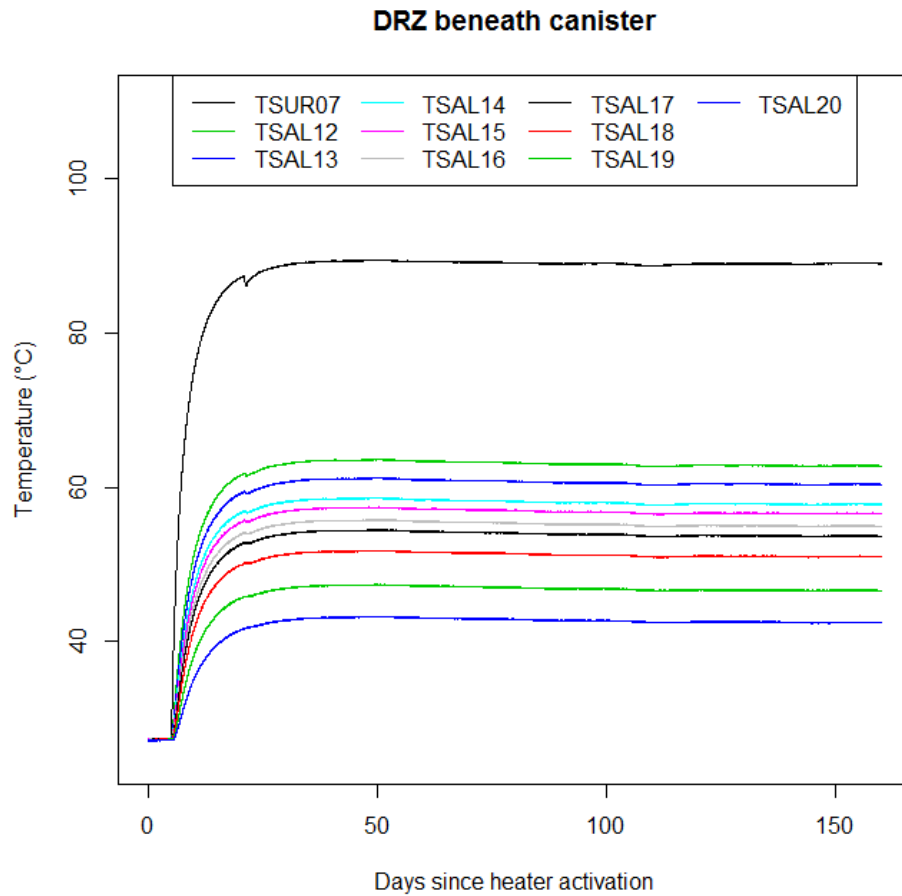


Figure 16: Temperature measurements for transect extending vertically beneath canister. Thermocouple labels are shown as in Figure 12.

Figure 17 shows the temperature gradient along the thermocouple arrays above and lateral to the canister. Temperature profiles are similar in all directions, indicating similar conductive heat transfer and comparable material properties throughout the pile.

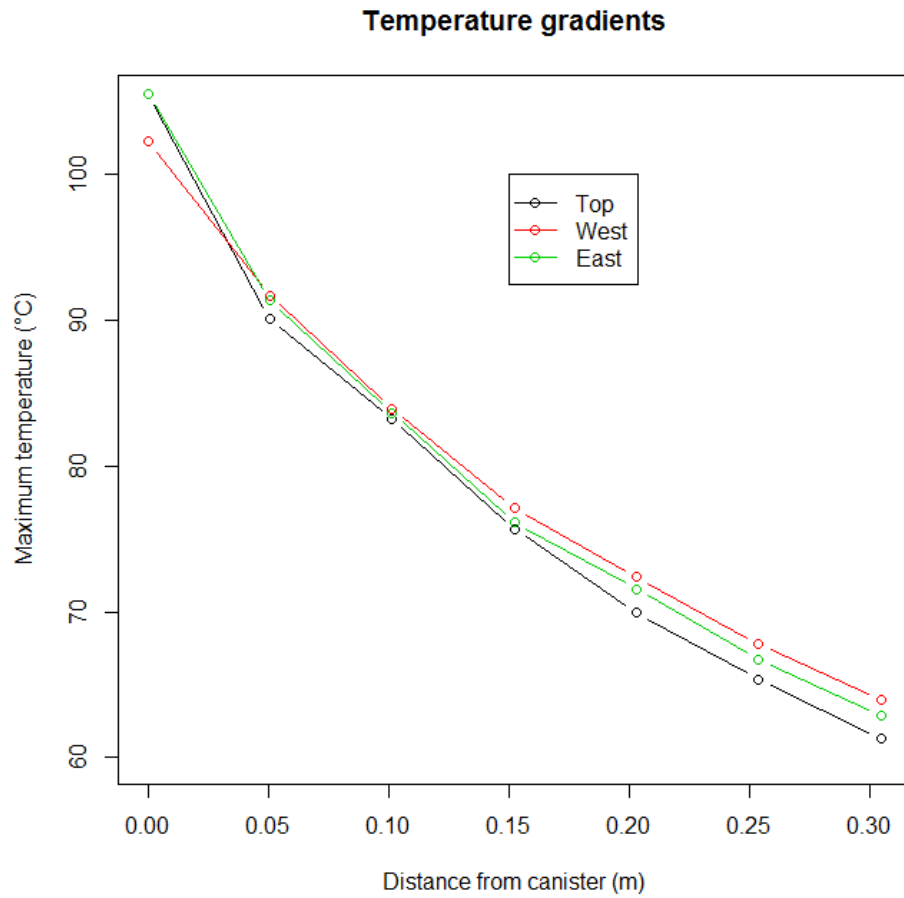


Figure 17: Temperature transects for pile top (black), west (red, left on Figures 10 and 12), and east (green, right on Figures 10 and 12).

Notes collected during experiment**01/23/2018****Shawn Otto****Testing of a Prototype Canister Heater in the WIPP Underground (non-qa/information only)**

Per the request of LANL modelers, air temperature measurements were made at specified locations (see tables and photo) in the Air Intake Shaft drift of the WIPP underground where the PCH is located. A Fluke 53/54 II B meter with type K thermocouples was used to make the measurements. The Fluke had 2 type K thermocouples for measuring temperature and the average of the 2 thermocouples were documented. The thermocouples were located at the specified locations and between 15 -30 seconds were needed until the measurements stabilized. The Michell chilled mirror hygrometer, that measures the environmental temperature for the PCH experiment, was used to document the environmental temperature that corresponds with the time that the Fluke temperature measurements were made.

Note that the environmental temperature measured with the chilled mirror is part of the data acquisition system. The following tables show the approximated location that the measurements were collected. The photo illustrates the locations described in the tables.

Experiments and Modeling to Support Field Test Design

Location #	Location Description	Date	Start Time	Fluke Temp, deg C	Chilled Mirror Env Temp, degC
1	mid PCH - top of salt pile	1/23/2018	815	24.7	24.3
2	mid PCH - mine back	1/23/2018	815	24.9	24.3
3	next to chilled mirror env temp sensor	1/23/2018	815	24.7	24.3
4	PCH pintel end - top of salt pile	1/23/2018	815	24.8	24.3
5	PCH pintel end - mine back	1/23/2018	815	24.8	24.3
1	mid PCH - top of salt pile	1/23/2018	1010	24.9	23.9
2	mid PCH - mine back	1/23/2018	1010	24.3	23.9
3	next to chilled mirror env temp sensor	1/23/2018	1010	24.0	23.9
4	PCH pintel end - top of salt pile	1/23/2018	1010	25.0	23.9
5	PCH pintel end - mine back	1/23/2018	1010	24.2	23.9
1	mid PCH - top of salt pile	1/23/2018	1133	25.2	24.1
2	mid PCH - mine back	1/23/2018	1133	24.8	24.1
3	next to chilled mirror env temp sensor	1/23/2018	1133	24.3	24.1
4	PCH pintel end - top of salt pile	1/23/2018	1133	25.0	24.1
5	PCH pintel end - mine back	1/23/2018	1133	24.8	24.1
Location #	Location Description	Height, ft	Distance from rib, ft		
1	mid PCH - top of salt pile	4.05	5.60		
2	mid PCH - mine back	9.60	10.50		
3	next to chilled mirror env temp sensor	6.60	1.75		
4	PCH pintel end - top of salt pile	4.45	3.45		
5	PCH pintel end - mine back	10.00	3.45		

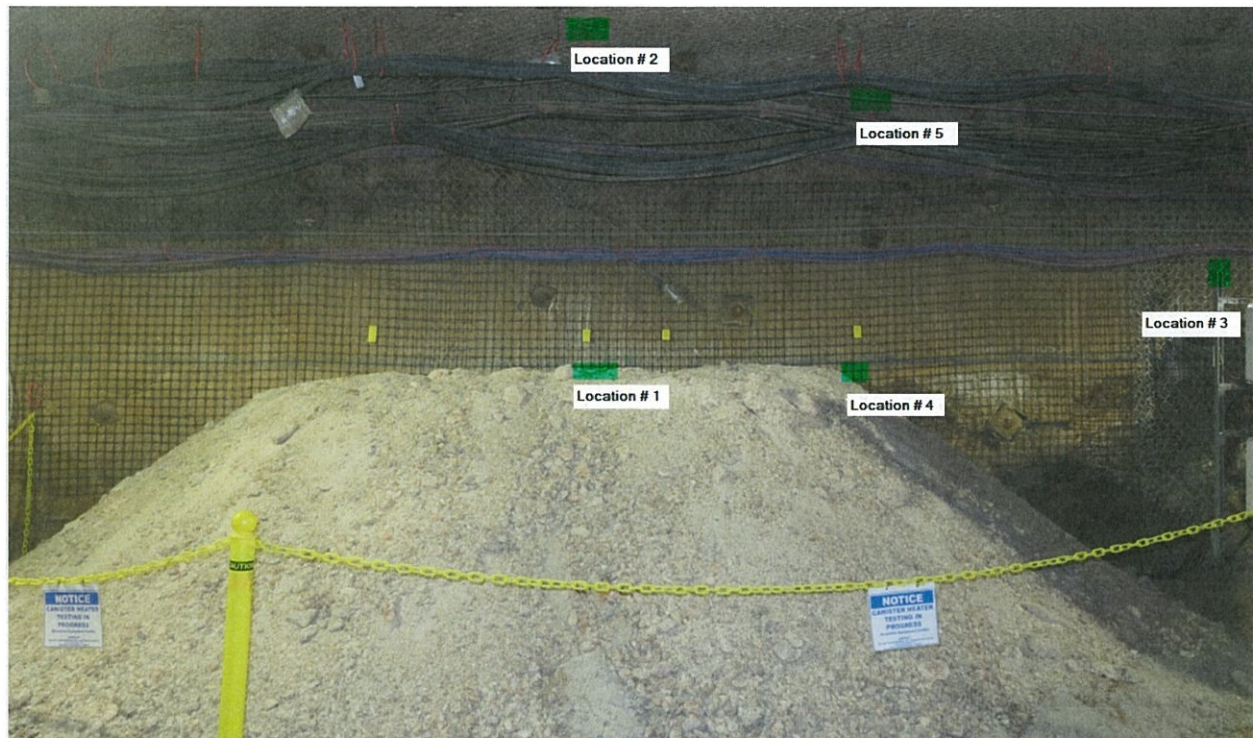


Figure 18: Location of temperature measurements

02/28/2018

Shawn Otto

Testing of a Prototype Canister Heater in the WIPP Underground (non-qa/information only)

Per the request of LANL modelers an evaluation of the ground was made near the prototype canister heater. The modelers are seeking information to help explain why the ground isn't getting as hot as the pre-model predicted.

The first evaluation consisting of using a scaling bar to sound the ground outside the ROM salt pile east of the experiment. Sounding of the ground showed no hollow ground and the ground is very solid.

Experiments and Modeling to Support Field Test Design

The second evaluation consisted of drilling a borehole with a 24" bit; which is the same bit used for the boreholes instrumented with thermocouples as described on page 103. The borehole was drilled at the midpoint of the canister approximately 8 to 10 inches east of the edge of the ROM salt pile. The drilling showed that the ground is very solid, no clay seams were encountered (all the salt emitting during the drilling process were white **in** color and no red were observed which is indicative of clay), and there were no voids encountered. Drilling were consistent throughout the 24 inches.

The borehole itself has a diameter of 15/16 inches and was approximately 24 inches deep. The following photographs depict visual reference for the aforementioned information. All of this information is being provided to the LANL modelers.

Experiments and Modeling to Support Field Test Design



Experiments and Modeling to Support Field Test Design

